

Model of incompressible turbulent flows via a kinetic theory

Ziyang Xin¹, Zhaoli Guo^{1, 2,†} and Hudong Chen^{3,‡}

¹State Key Laboratory of Coal Combustion, School of Energy and Power Engineering, Huazhong University of Science and Technology, Wuhan, 430074, China

²Institute of Interdisciplinary Research for Mathematics and Applied Science, Huazhong University of Science and Technology, Wuhan 430074, China

³College of Energy Engineering, Zhejiang University, Hangzhou 310027, China

Kinetic theory offers a promising alternative to conventional turbulence modelling by providing a mesoscopic perspective that naturally captures non-equilibrium physics such as non-Newtonian effects. In this work, we present an extension and theoretical analysis of the recent kinetic model for incompressible turbulent flows developed by Chen et al. (Atmos. 14(7), 1109, 2023), constructed for unbounded flows. The first extension is to reselect a relaxation time such that the turbulent transport coefficients are obtained more consistently and better align with well-established turbulence theory. The Chapman-Enskog (CE) analysis of the kinetic model reproduces the traditional linear eddy viscosity and gradient diffusion models for Reynolds stress and turbulent kinetic energy flux at the first order, and yields nonlinear eddy viscosity and closure models at the second order. Particularly, a previously unreported CE solution for turbulent kinetic energy flux is obtained. The second extension is to enable the model for wall-bounded turbulent flows with preserved near-wall asymptotic behaviours. This involves developing a low-Reynolds-number kinetic model incorporating wall damping effects and viscous diffusion, with boundary conditions enabling both viscous sublayer resolution and wall function application. Comprehensive validation against experimental and DNS data for turbulent plane Couette flow demonstrates excellent agreement in predicting mean velocity profiles, skin friction coefficients, and Reynolds stress distributions. It reveals that an averaged turbulent flow behaves similarly to a rarefied gas flow at a finite Knudsen number, capturing non-Newtonian effects inaccessible to linear eddy viscosity models. This kinetic model provides a physics-based foundation for turbulence modelling with reduced empirical dependence.

1. Introduction

Incompressible turbulent flows are ubiquitous in nature and engineering, occurring in systems ranging from atmospheric and oceanic flows to industrial processes, yet their inherent complexity continues to challenge predictive modelling efforts (Pope 2001). Although advances in high-performance computing have greatly expanded the scope of direct numerical simulation (DNS) of the Navier–Stokes (NS) equations (Moin & Mahesh 1998), the computational cost of fully resolving turbulent flows remains prohibitive, particularly at high Reynolds numbers and in complex geometries. Consequently, considerable effort has been devoted to turbulence modelling based on statistically averaged equations, aiming to capture key features of turbulent flows such as the mean velocity profile and the root mean square velocity fluctuations.

Among statistically averaged equations, the Reynolds averaged Navier–Stokes (RANS) equations (Reynolds 1895), obtained by time averaging the incompressible NS equations, remain

† Email address for correspondence: zlguo@hust.edu.cn

‡ Email address for correspondence: hdc25@zju.edu.cn

the most widely used framework in turbulence modelling. A central challenge in applying the RANS equations is to devise closure models that approximate the Reynolds stress and scalar flux introduced by the averaging process. One of the earliest closure models, the Prandtl mixing length hypothesis introduces the concept of eddy viscosity by drawing an analogy between turbulent mixing and molecular momentum transport (Prandtl 1925). To this day, eddy viscosity concepts remain a cornerstone of turbulence theory and engineering modelling. The linear eddy viscosity closure for Reynolds stress with gradient diffusion closure for scalar flux (Lauder & Spalding 1983; Spalart & Allmaras 1992; Menter 1997; Wilcox 2008) and nonlinear extensions (Pope 1975; Speziale 1987; Gatski & Speziale 1993; Craft *et al.* 1996; Wallin & Johansson 2000) that incorporate strain and rotation tensor invariants, have achieved success across different flow types, yet they typically rely on *ad hoc* parameters that require empirical specification (Durbin 2018). The pursuit of more sophisticated closure strategies has resulted in Reynolds stress transport models that directly solve the governing equations for individual Reynolds stress tensor components, providing the ability to capture secondary flow structures and the lag phenomena between a rapidly changing applied strain rate and the response (Lauder *et al.* 1975; Yakhot *et al.* 1992; Hamlington & Dahm 2008). However, these higher-order closure models introduce challenges related to the uncertain physical foundations of the required higher-order turbulence correlations and the specification of appropriate boundary conditions.

Although eddy viscosity models have achieved considerable success in RANS frameworks, they are fundamentally limited by the assumption of scale separation between the mean and fluctuating flow fields (Monin & Yaglom 2013). This limitation can be naturally addressed by seeking a description in terms of kinetic theory for gas molecules, as kinetic equations do not rely on such scale separation assumptions (Cercignani 1988). Building on this kinetic perspective, Chen *et al.* (2003) introduced an extended Boltzmann kinetic framework, in which turbulent fluctuations are treated analogously to molecular thermal fluctuations. Their formulation circumvents the scale separation assumption inherent in classical eddy viscosity models, naturally recovering Reynolds stress and higher-order (nonlinear and non-Newtonian) corrections through Chapman–Enskog (CE) expansion (Chapman & Cowling 1990), with all model coefficients consistently determined from kinetic theory. Furthermore, by analogy, a Fokker–Planck equation explicitly tailored for turbulence modelling was developed by Heinz (2007) and Luan *et al.* (2025). Using the CE expansion, Luan *et al.* (2025) derived a nonlinear eddy viscosity model from this Fokker–Planck formulation, which closely aligns with the results of the Bhatnagar–Gross–Krook (BGK) model of Chen *et al.* (2004), differing primarily in the omission of the molecular viscous term. Encouragingly, their results demonstrate that the resulting quadratic eddy viscosity model outperforms the existing linear eddy viscosity model and achieves comparable accuracy to cubic eddy viscosity models for two-dimensional flows, without resorting to *ad hoc* parameters in the Reynolds stress constitutive relation (Luan *et al.* 2025). However, no theoretical analysis or numerical simulation has yet been reported that solves these kinetic models directly. A key drawback of these kinetic models is that they impose turbulence by analogy, replacing molecular thermal fluctuations with turbulent fluctuations, without deriving a description of the turbulence dynamics from the first principles.

Another strategy is to develop kinetic models for turbulence directly from the Boltzmann equation by systematically eliminating small-scale fluctuations through successive averaging procedures. Chen *et al.* (1999) applied renormalization group techniques to the Boltzmann–BGK equation (Bhatnagar *et al.* 1954) to develop a subgrid-scale viscosity model (SGS). Subsequently, Ansumali *et al.* (2004) constructed a turbulence model using a mean-field approach to filter SGS effects, establishing connections with the Smagorinsky-type closures. Girimaji (2007) further formulated a Boltzmann kinetic equation by incorporating SGS closure to characterize filtered turbulent flows, applicable to both continuum and non-continuum effects. Recently, Yang & Xu (2025) developed the wave-particle turbulence simulation method, which conjectured and

numerically showed that kinetic representations may be advantageous in describing turbulent non-equilibrium physics. However, a fundamental limitation arises because the averaged equilibrium distribution retains the thermodynamic temperature in the same functional role as turbulent kinetic energy. This prevents the systematic removal of molecular thermal effects through successive averaging processes, resulting in eddy viscosity formulations that exhibit unphysical dependence on molecular temperature rather than being determined solely by turbulent flow characteristics. This limitation highlights fundamental difficulties in applying the conventional Boltzmann equation to turbulence modelling and suggests the need for alternative approaches to statistical averaging.

[Lundgren \(1967\)](#) derived an infinite hierarchy of equations for the multi-point velocity distribution function (VDF) of fluid elements, starting from the incompressible NS equations. In this hierarchy, the n th equation contains an unknown $(n + 1)$ -point VDF, closely resembling the Bogoliubov-Born-Green-Kirkwood-Yvon (BBGKY) ([Cohen & Balazs 1962](#)) hierarchy for multi-particle VDF in kinetic theory. The Boltzmann equation for short-range interacting particles and the Fokker-Planck equation for long-range Coulomb interactions are derived from the BBGKY hierarchy through appropriate closure approximations. In subsequent work, [Lundgren \(1969\)](#) attempted to close the system at the one-point level by employing a relaxation model identical in form to the BGK model. The resulting equation was solved for several idealized problems without solid boundaries, and good agreement with available experiments was found. [Srinivasan et al. \(1977\)](#) extended the work of [Lundgren \(1969\)](#) to turbulent flows bounded by solid walls, developing two types of boundary conditions based on the wall function method and employing the discrete ordinate method for numerical solution. However, due to the restriction to regions outside the viscous sublayer, the near-wall Reynolds shear stress was overpredicted, leading to an incorrect shear-stress profile. Lundgren's model equation provides a very good description of turbulence for the flow situations considered and offers an analytical tool for further study of more complex turbulent flows; yet to our knowledge, this approach has not been pursued in subsequent turbulence research. [Chen et al. \(2023, 2024\)](#) take a different approach but arrives at a similar BGK-type model for the VDF. Their analysis is developed from the idea of Klimontovich-type kinetic equation ([Klimontovich 1969](#)) for fluid elements, which exactly satisfies the incompressible NS equations. Averaging the Klimontovich equation leads to a BGK-type equation without suffering from the mixing of dynamic scales with the thermodynamic temperature. Unlike the model of [Lundgren \(1969\)](#), the dissipation rate is incorporated into the collision term rather than added through a source term, providing a more physically realistic representation of dissipation in eddy collisions. These studies provide a rigorous kinetic approach for turbulence modelling, moving beyond heuristic analogies to offer fundamental insights into turbulent fluctuation dynamics and their macroscopic effects. Although the kinetic model developed by [Chen et al. \(2023\)](#) provides a rigorous theoretical foundation for turbulence modelling, two critical limitations remain. First, the CE analysis for the Reynolds stress is based on the results of the BGK model that does not properly incorporate dissipation of turbulent kinetic energy ([Chen et al. 2004](#)), causing the relaxation time estimation by [Chen et al. \(2024\)](#) to produce unrealistically high turbulent Prandtl number and higher-order transport coefficients. Second, the model was constructed for unbounded fully developed turbulent flows, and suitable near-wall treatment for wall-bounded turbulence remains to be developed.

The aim of this study is to extend, analyze, and validate the kinetic model developed by [Chen et al. \(2023\)](#). Through Chapman-Enskog expansion, we derive eddy viscosity and gradient diffusion models with transport coefficients determined from kinetic theory principles, reducing reliance on *ad hoc* parameters. The theoretical results are validated through detailed comparison with experimental data and direct numerical simulations of turbulent plane Couette flow. The remainder of the paper is organized as follows. §2 presents the kinetic model for incompressible turbulence. In §3, we establish connections with traditional eddy viscosity models and compare

the transport coefficients. §4 presents an extension of the model to wall-bounded turbulence. In §5, we validate the models through turbulent Couette flow simulations, and §6 provides concluding remarks.

2. Kinetic model for incompressible turbulence

2.1. Kinetic Representation of incompressible turbulence

Rather than relying on the ensemble-averaged Boltzmann equation originally devised for molecular gases, [Chen et al. \(2023\)](#) provides a comprehensive kinetic representation of incompressible turbulence at both the NS (fluid elements) level and the RANS (eddies) level. They first introduced a Klimontovich-type kinetic equation for fluid elements,

$$\partial_t f + \boldsymbol{\xi} \cdot \nabla f + \boldsymbol{a} \cdot \nabla_{\boldsymbol{\xi}} f = 0, \quad \boldsymbol{a} = -\nabla p + \nu_0 \nabla^2 \boldsymbol{u}, \quad (2.1)$$

where $f \equiv f(\boldsymbol{x}, \boldsymbol{\xi}, t)$ is the velocity distribution function (VDF) for fluid elements with velocity $\boldsymbol{\xi} \equiv (\xi_x, \xi_y, \xi_z)$ at position $\boldsymbol{x} \equiv (x, y, z)$ and time t . ∇ and $\nabla_{\boldsymbol{\xi}}$ are the gradient operators in physical and velocity spaces, respectively. ν_0 is the molecular viscosity, p is the pressure determined by the incompressibility constraint, and the fluid velocity \boldsymbol{u} is defined by

$$\boldsymbol{u} = \int \boldsymbol{\xi} f d\boldsymbol{\xi}, \quad (2.2)$$

and $\int f d\boldsymbol{\xi} = 1$ for an incompressible flow. Taking the zeroth and first order moments of (2.1), we obtain

$$\begin{aligned} \nabla \cdot \boldsymbol{u} &= 0, \\ \partial_t \boldsymbol{u} + (\boldsymbol{u} \cdot \nabla) \boldsymbol{u} &= -\nabla p + \nu_0 \nabla^2 \boldsymbol{u}, \end{aligned} \quad (2.3)$$

which exactly reproduces the NS equations at the hydrodynamic level.

Subsequently, applying ensemble averaging to the kinetic equation (2.1) provides the kinetic description of the incompressible mean turbulent field:

$$\partial_t F + \boldsymbol{\xi} \cdot \nabla F + \bar{\boldsymbol{a}} \cdot \nabla_{\boldsymbol{\xi}} F = C, \quad (2.4)$$

where $F \equiv F(\boldsymbol{x}, \boldsymbol{\xi}, t) = \langle f(\boldsymbol{x}, \boldsymbol{\xi}, t) \rangle$ is an ensemble averaged VDF, with $\langle \cdot \rangle$ denoting the ensemble average. $C \equiv -\nabla_{\boldsymbol{\xi}} \cdot \langle \boldsymbol{a}' f' \rangle$ is the collision operator, with \boldsymbol{a}' and f' denoting the fluctuating components of \boldsymbol{a} and f , respectively. According to the linearity and incompressibility, the external force $\bar{\boldsymbol{a}}$ is given as

$$\bar{\boldsymbol{a}} = \langle \boldsymbol{a} \rangle = -\nabla \bar{p} + \nu_0 \nabla^2 \boldsymbol{U}, \quad (2.5)$$

where ν_0 is the molecular viscosity, $\bar{p} = \langle p \rangle$ and $\boldsymbol{U} = \langle \boldsymbol{u} \rangle$ are the mean (ensemble averaged) pressure and velocity, respectively. The mean pressure distribution is governed by the mean velocity field according to the constraint $\nabla^2 \bar{p} = -\nabla \nabla : \boldsymbol{U} \boldsymbol{U} - \nabla \nabla : (\langle \boldsymbol{u}' \boldsymbol{u}' \rangle)$.

The collision operator C satisfies conservation of mass and momentum,

$$\int C d\boldsymbol{\xi} = 0, \quad \int \boldsymbol{\xi} C d\boldsymbol{\xi} = 0. \quad (2.6)$$

But the collision is not conservative with respect to energy, entailing energy dissipation,

$$\frac{1}{2} \int (\boldsymbol{\xi} - \boldsymbol{U})^2 C d\boldsymbol{\xi} = -\epsilon, \quad (2.7)$$

where ϵ is the dissipation rate. Therefore, the ensemble averaged Klimontovich-type equation (2.4) can be regarded as a Boltzmann equation from the kinetic perspective, describing the transport and collision of eddy.

Mean quantities, such as the mean velocity \boldsymbol{U} , turbulent kinetic energy (TKE) K , Reynolds

stress tensor σ and turbulent kinetic energy flux Q , can be obtained by integrating the ensemble averaged VDF over the velocity space, i.e.

$$\begin{aligned} U &= \langle \mathbf{u} \rangle = \int \xi F d\xi, \\ K &= \frac{1}{2} \langle (\mathbf{u}')^2 \rangle = \frac{1}{2} \int (\xi - U)^2 F d\xi, \\ \sigma &= -\langle \mathbf{u}' \mathbf{u}' \rangle = - \int (\xi - U)(\xi - U) F d\xi, \\ Q &= \frac{1}{2} \langle \mathbf{u}' (\mathbf{u}')^2 \rangle = \frac{1}{2} \int (\xi - U)(\xi - U)^2 F d\xi, \end{aligned} \quad (2.8)$$

where $\int F d\xi = 1$, corresponding to the normalization of the VDF for incompressible flow.

The well-known incompressible RANS equations can be obtained by taking the moments of the kinetic equation (2.4),

$$\begin{aligned} \nabla \cdot \mathbf{U} &= 0, \\ \partial_t \mathbf{U} + (\mathbf{U} \cdot \nabla) \mathbf{U} &= -\nabla \bar{p} + \nu_0 \nabla^2 \mathbf{U} + \nabla \cdot \boldsymbol{\sigma}, \\ \partial_t K + (\mathbf{U} \cdot \nabla) K &= -\nabla \cdot \mathbf{Q} + \boldsymbol{\sigma} : \mathbf{S} - \epsilon, \end{aligned} \quad (2.9)$$

where $\mathbf{S} = \frac{1}{2} [\nabla \mathbf{U} + (\nabla \mathbf{U})^T]$ is the rate of strain tensor. It can be seen that K , $\boldsymbol{\sigma}$, and \mathbf{Q} are completely determined by the solution of the averaged kinetic equation without any assumptions in this kinetic representation.

2.2. BGK model for average turbulence dynamics

Since the collision term lacks an explicit form in terms of the averaged variables, one needs to find an appropriate closure in the above kinetic representation. Interestingly, the asymptotic limit of the collision process C assumes a Gaussian form based on semi-theoretical arguments (Chen et al. 2023), which is also consistent with experimental observations in homogeneous turbulent flows where the one-point VDF exhibits a local Gaussian form (Tavoularis & Corrsin 1981; Sreenivasan & Yakhot 2021; Sreenivasan et al. 2024). As a result, Chen et al. (2023) modeled the collision term C as a relaxation process toward the local Gaussian equilibrium with a relaxation time τ , namely, a BGK form,

$$C(F) = \frac{F^{eq} - F}{\tau}, \quad (2.10)$$

where F^{eq} is the equilibrium VDF,

$$F^{eq} = \left(\frac{4}{3} \pi K^{eq} \right)^{-3/2} \exp \left[-\frac{3(\xi - U)^2}{4K^{eq}} \right], \quad (2.11)$$

where K^{eq} is the equilibrium TKE. Compared with the canonical Maxwell equilibrium distribution, TKE assumes a role analogous to temperature in classical molecular thermodynamics. In fact, F^{eq} represents a Gaussian equilibrium distribution that excludes the non-trivial flow-induced fluctuations present in F ; the latter possesses non-Gaussian properties (Frisch 1996) such as flatness and skewness.

Based on the properties of the collision term, one can obtain

$$\begin{aligned} \int F^{eq} d\xi &= \int F d\xi = 1, \\ \int \xi F^{eq} d\xi &= \int \xi F d\xi = U, \end{aligned} \quad (2.12)$$

and

$$\int \frac{(\xi - \mathbf{U})^2}{2} \frac{F^{eq} - F}{\tau} d\xi = \frac{K^{eq} - K}{\tau} = -\epsilon, \quad (2.13)$$

and we have the equilibrium TKE $K^{eq} = K - \tau\epsilon$ according to (2.13).

For the relaxation time, [Chen et al. \(2024\)](#) provide a theoretical estimation of $\tau = C_\tau K/\epsilon$ with $C_\tau = 6/7$ based on the fluctuation-dissipation theorem that is absent in purely hydrodynamic approaches for stationary, homogeneous and isotropic turbulent flows. It also determines the turbulent viscosity, turbulent Prandtl number, and all higher-order transport coefficients involved in σ and \mathbf{Q} by an effective finite Knudsen number expansion. They obtain the turbulent viscosity $\nu_T = 2\tau K^{eq}/3 = 2C_\tau(1 - C_\tau)K^2/(3\epsilon)$ based on the CE analysis of the BGK model that does not properly incorporate dissipation of TKE ([Chen et al. 2004](#)). This leads to unrealistically high turbulent Prandtl number and higher-order transport coefficients (See §3.2). Since turbulent viscosity exhibits a quadratic dependence on the coefficient C_τ , we can select the another root instead of the original one:

$$\tau = \frac{1}{7} \frac{K}{\epsilon}. \quad (2.14)$$

This choice yields the same viscosity as derived by [Chen et al. \(2024\)](#), while providing more reasonable turbulent Prandtl number and improved higher-order transport coefficients. This coefficient is also very close to the value 1/6 suggested by [Lundgren \(1969\)](#), who assumed the relaxation time to scale as $\tau \sim L/\sqrt{K}$ where L is the integral length scale of turbulence (defined through $\epsilon = K^{3/2}/L$).

In the end, the dissipation rate ϵ remains an unspecified quantity, requiring an additional scale equation to determine its evolution. The most straightforward approach is to adopt an established formulation from conventional turbulence models (e.g., the $K - \epsilon$ model) to prescribe the evolution equation for ϵ . Alternatively, the conventional $K - \omega$ turbulence models can also be utilized, where the relaxation time is expressed as $\tau \sim 1/\omega$, with $\omega \sim \epsilon/K$ being the specific dissipation rate ([Wilcox 1998](#)). However, these formulations remain incomplete from the perspective of kinetic theory, as they still depend on externally specified parameters. Therefore, a fully self-consistent kinetic theoretic description for inhomogeneous statistical turbulence would be an ultimate goal.

3. Connection with traditional eddy viscosity models

3.1. Chapman-Enskog analysis

As mentioned in the Introduction, almost all traditional turbulence closures, including the eddy viscosity and gradient diffusion models, aim to approximate the Reynolds stress σ and the TKE flux \mathbf{Q} by the mean variables \mathbf{U} and K in the RANS equations. This hydrodynamic description can be derived by looking for a normal solution to the kinetic equation (2.4) with the BGK collision term (2.10) by means of the CE expansion technique ([Chapman & Cowling 1990](#)). We first use a reference velocity U_{ref} , reference collision time τ_{ref} and reference length L_{ref} to non-dimensionalise the kinetic equation (2.4),

$$\frac{\partial \hat{F}}{\partial \hat{t}} + \hat{\xi} \cdot \frac{\partial \hat{F}}{\partial \hat{x}} + \left(-\frac{\partial \hat{p}}{\partial \hat{x}} + \frac{1}{Re} \hat{\nabla}^2 \hat{\mathbf{U}} \right) \cdot \frac{\partial \hat{F}}{\partial \hat{\xi}} = \frac{1}{\mathcal{K}} \frac{\hat{F}^{eq} - \hat{F}}{\hat{\tau}}, \quad (3.1)$$

where $Re = U_{ref}L_{ref}/\nu_0$ is the Reynolds number (Re), and $\mathcal{K} = U_{ref}\tau_{ref}/L_{ref}$ can be interpreted as a turbulence-based Knudsen number that quantifies the ratio of unresolved to resolved flow scales ([Luan et al. 2025](#)). Notably, it vanishes when returning to the dimensional form. For simplicity, the caret indicating non-dimensional quantities will be omitted hereafter. If \mathcal{K} is regarded as a small parameter, the VDF deviations from equilibrium can be expanded in

powers of \mathcal{K} as

$$F = F^{(0)} + \mathcal{K}F^{(1)} + \mathcal{K}^2F^{(2)} + \dots, \quad (3.2)$$

where $F^{(0)} = F^{eq}$. Correspondingly, the temporal and spatial derivatives are also expanded formally as

$$\partial_t = \mathcal{K}\partial_{t_1} + \mathcal{K}^2\partial_{t_2} + \dots, \quad \nabla = \mathcal{K}\nabla_1, \quad (3.3)$$

and the force and strain rate are similarly expanded as

$$\begin{aligned} \bar{\mathbf{a}} &= \mathcal{K}\bar{\mathbf{a}}^{(1)} + \mathcal{K}^2\bar{\mathbf{a}}^{(2)}, \quad \bar{\mathbf{a}}^{(1)} = -\nabla_1\bar{p}, \quad \bar{\mathbf{a}}^{(2)} = \nu_0\nabla_1^2\mathbf{U}, \\ \mathbf{S} &= \mathcal{K}\mathbf{S}^{(1)}, \quad \mathbf{S}^{(1)} = \frac{1}{2}\left(\nabla_1\mathbf{U} + (\nabla_1\mathbf{U})^T\right). \end{aligned} \quad (3.4)$$

Taking the velocity moments of the expanded VDF (3.2), the expressions of K , σ and \mathbf{Q} can be written as

$$\begin{aligned} K &= K^{(0)} + \mathcal{K}K^{(1)} + \mathcal{K}^2K^{(2)} + \dots, \\ \sigma &= \sigma^{(0)} + \mathcal{K}\sigma^{(1)} + \mathcal{K}^2\sigma^{(2)} + \dots, \\ \mathbf{Q} &= \mathbf{Q}^{(0)} + \mathcal{K}\mathbf{Q}^{(1)} + \mathcal{K}^2\mathbf{Q}^{(2)} + \dots. \end{aligned} \quad (3.5)$$

The detailed expansions and formulas at each order are provided in Appendix A. In particular, the zeroth-order approximation of TKE, Reynolds stress and TKE flux can be determined by taking moments of F^{eq} ,

$$\begin{aligned} K^{(0)} &= K^{eq}, \\ \sigma^{(0)} &= -\frac{2}{3}K^{eq}\mathbf{I}, \\ \mathbf{Q}^{(0)} &= 0, \end{aligned} \quad (3.6)$$

where \mathbf{I} is the unit tensor. Note that $\sigma^{(0)}$ involves K^{eq} rather than K , so it does not represent the isotropic portion of the Reynolds stress.

The first-order approximation can be obtained as

$$\begin{aligned} \sigma^{(1)} &= -\frac{2}{3}K^{(1)}\mathbf{I} + \frac{4\tau K^{eq}}{3}\mathbf{S}^{(1)}, \\ \mathbf{Q}^{(1)} &= -\frac{10\tau K^{eq}}{9}\nabla_1K^{eq}. \end{aligned} \quad (3.7)$$

Truncating to first order recovers the linear eddy viscosity model for the Reynolds stress and gradient diffusion model for TKE flux,

$$\begin{aligned} \sigma &\approx \sigma^{(0)} + \mathcal{K}\sigma^{(1)} = -\frac{2K}{3}\mathbf{I} + 2\nu_T\mathbf{S}, \\ \mathbf{Q} &\approx \mathbf{Q}^{(0)} + \mathcal{K}\mathbf{Q}^{(1)} = -\frac{\nu_T}{\text{Pr}_T}\nabla K, \end{aligned} \quad (3.8)$$

with $K \approx K^{(0)} + \mathcal{K}K^{(1)}$, and the turbulent viscosity ν_T and turbulent Prandtl number Pr_T are given by

$$\nu_T = \frac{2\tau K^{eq}}{3}, \quad \text{Pr}_T = \frac{3K}{5K^{eq}}. \quad (3.9)$$

The next order contributions to σ and Q are obtained as

$$\begin{aligned}\sigma^{(2)} &= -\frac{2K^{(2)}}{3}\mathbf{I} - \frac{4\tau}{3K^{eq}}(\partial_{t1} + \mathbf{U} \cdot \nabla_1) [\tau(K^{eq})^2 \mathbf{S}^{(1)}] \\ &\quad - \frac{8\tau^2 K^{eq}}{3} \left[\mathbf{S}^{(1)} \cdot \mathbf{S}^{(1)} - \frac{1}{3}(\mathbf{S}^{(1)} : \mathbf{S}^{(1)})\mathbf{I} \right] + \frac{4\tau^2 K^{eq}}{3} \left(\mathbf{S}^{(1)} \cdot \boldsymbol{\Omega}^{(1)} - \boldsymbol{\Omega}^{(1)} \cdot \mathbf{S}^{(1)} \right) \\ &\quad - \frac{4\tau}{9} \left[\nabla_1 (\tau K^{eq} \nabla_1 K^{eq}) + (\nabla_1 (\tau K^{eq} \nabla_1 K^{eq}))^T - \frac{2}{3} \nabla_1 \cdot (\tau K^{eq} \nabla_1 K^{eq}) \mathbf{I} \right], \\ Q^{(2)} &= \frac{10\tau}{9K^{eq}}(\partial_{t1} + \mathbf{U} \cdot \nabla_1) [\tau(K^{eq})^2 \nabla_1 K^{eq}] + \frac{10\tau^2 K^{eq}}{9} (\nabla_1 K^{eq}) \cdot (\nabla_1 \mathbf{U})^T \\ &\quad - \frac{5\tau K^{eq}}{3} \nabla_1 \cdot \left(\frac{4\tau K^{eq}}{3} \mathbf{S}^{(1)} \right) + \frac{5\tau K^{eq}}{3} \mathbf{a}^{(1)},\end{aligned}\tag{3.10}$$

where $\boldsymbol{\Omega} = \frac{1}{2} [\nabla \mathbf{U} - (\nabla \mathbf{U})^T]$ is the vorticity tensor of the mean velocity field. The second-order expansion, as shown in (3.10), provides a more accurate representation of the Reynolds stress and TKE flux. These higher-order effects, consistent with classical turbulence theory, are crucial for capturing complex turbulent behaviours such as secondary flow structures and flows subject to sudden distortions (Chen et al. 2004). The second-order TKE flux term is analogous to the Burnett heat flux in rarefied flow that can describe non-Fourier heat transfer phenomena (counter-gradient heat flux) (Venugopal et al. 2019). It could also be a potential responsible for some of the observed counter-gradient diffusion phenomena of TKE in buoyant flows (Grötzbach 1982; Moeng & Wyngaard 1989; Chandra & Grötzbach 2007).

Truncating to second order, the TKE is expressed as

$$K \approx K^{eq} + \mathcal{K} K^{(1)} + \mathcal{K}^2 K^{(2)}.\tag{3.11}$$

Based on the assumption that $\partial_t \approx \mathcal{K} \partial_{t1}$, the Reynolds stress and the TKE flux can be approximated as

$$\begin{aligned}\sigma &\approx \sigma^{(0)} + \mathcal{K} \sigma^{(1)} + \mathcal{K}^2 \sigma^{(2)} \\ &= -\frac{2K}{3}\mathbf{I} + 2\nu_T \mathbf{S} - \frac{\tau}{K^{eq}} \frac{D}{Dt} [2\nu_T K^{eq} \mathbf{S}] - \frac{6\nu_T^2}{K^{eq}} \left[\mathbf{S} \cdot \mathbf{S} - \frac{1}{3}(\mathbf{S} : \mathbf{S})\mathbf{I} \right] + \frac{3\nu_T^2}{K^{eq}} (\mathbf{S} \cdot \boldsymbol{\Omega} - \boldsymbol{\Omega} \cdot \mathbf{S}) \\ &\quad - \frac{2\nu_T}{3K^{eq}} \left[\nabla (\tau K^{eq} \nabla K^{eq}) + (\nabla (\tau K^{eq} \nabla K^{eq}))^T - \frac{2}{3} \nabla \cdot (\tau K^{eq} \nabla K^{eq}) \mathbf{I} \right], \\ Q &\approx Q^{(0)} + \mathcal{K} Q^{(1)} + \mathcal{K}^2 Q^{(2)} \\ &= -\frac{\nu_T}{Pr_T} \nabla K + \frac{\tau}{K^{eq}} \frac{D}{Dt} \left[\frac{\nu_T}{Pr_T} K^{eq} \nabla K \right] + \frac{5\nu_T^2}{2K^{eq}} (\nabla K^{eq}) \cdot (\nabla \mathbf{U})^T - \frac{5\nu_T}{2} \nabla \cdot (2\nu_T \mathbf{S}) - \frac{5\nu_T}{2} \nabla \bar{p},\end{aligned}\tag{3.12}$$

where $D/Dt \equiv \partial_t + \mathbf{U} \cdot \nabla$ is the material derivative along the mean velocity field. The linear eddy viscosity model (3.8) is in close agreement with the results obtained from traditional kinetic equations for turbulent flow (such as the Boltzmann-BGK model that does not involve TKE dissipation (Chen et al. 2004) and the Fokker-Planck equation (Heinz 2007; Luan et al. 2025)). In contrast, the nonlinear results (3.12) derived from the present model yield different material derivative of \mathbf{S} and higher-order derivative terms of TKE. Additionally, we have derived both the gradient diffusion model and its nonlinear counterpart, which are rarely modeled in conventional turbulence models.

The material derivative in (3.12) is both interesting and revealing. Considering only the linear

closures with respect to S and ∇K in equation (3.12), we have

$$\phi \approx \phi^{lin} - \frac{\tau}{K^{eq}} \frac{D(K^{eq}\phi^{lin})}{Dt} = \left(1 - \frac{\tau}{K^{eq}} \frac{DK^{eq}}{Dt}\right) \phi^{lin} - \tau \frac{D\phi^{lin}}{Dt}, \quad (3.13)$$

where $\phi = \sigma$ or $\phi = Q$, whose linear parts ϕ^{lin} are $2\nu_T S$ and $-\frac{\nu_T}{Pr_T} \nabla K$, respectively. First, we find that the effect of a finite relaxation time τ implies that the stress and TKE flux are not simply determined by the immediate local ϕ^{lin} , but rather emerge from the history of ϕ^{lin} at an earlier moment and at a location further upstream in the flow, that is,

$$\phi \approx \left(1 - \frac{\tau}{K^{eq}} \frac{DK^{eq}}{Dt}\right) \phi^{lin}(x - \mathbf{U}\tau^*, t - \tau^*), \quad \tau^* = \frac{\tau}{1 - \frac{\tau}{K^{eq}} \frac{DK^{eq}}{Dt}}. \quad (3.14)$$

This memory effect could be responsible for the turbulent phenomena seen in rapid distortion processes (Yakhot et al. 1992; Hamlington & Dahn 2008). Furthermore, the correction coefficient incorporates the local departure from the production-dissipation balance through the material derivative DK^{eq}/Dt . This non-equilibrium adjustment could address the well-documented overprediction of K and ϵ by classical linear closures in scenarios involving sustained energy injection, such as homogeneous shear turbulence (Yoshizawa & Nisizima 1993). Moreover, the “renormalized” relaxation time τ^* can also correct the unrealistically fast anisotropy decay predicted by $\tau = C_\tau K/\epsilon$ with C_τ being a constant in homogeneous turbulence (Lundgren 1969). Naturally, for flows characterized by slow spatial and temporal variations, these effects can be neglected, recovering the conventional eddy viscosity model.

3.2. Comparison of the transport coefficients

In this subsection, we conduct a comparison of the transport coefficients derived from the kinetic model under various relaxation time formulations with those obtained from the conventional $K - \epsilon$ models and quadratic nonlinear eddy viscosity models documented in the literature. For the $K - \epsilon$ model, the Reynolds stress and TKE flux are given by

$$\sigma = -\frac{2K}{3} \mathbf{I} + 2\nu_T S, \quad Q = -\frac{\nu_T}{Pr_T} \nabla K, \quad (3.15)$$

with

$$\nu_T = C_\mu \frac{K^2}{\epsilon}. \quad (3.16)$$

For the present choice of $\tau = K/(7\epsilon)$, we find

$$C_\mu = 0.0816, \quad Pr_T = 0.7; \quad (3.17)$$

On the other hand, the choice of $\tau = 6K/(7\epsilon)$ (Chen et al. 2024) gives

$$C_\mu = 0.0816, \quad Pr_T = 4.2; \quad (3.18)$$

For comparison, we list the corresponding values from two most representative $K - \epsilon$ models: the standard $K - \epsilon$ model (Lauder & Spalding 1983) gives

$$C_\mu = 0.09, \quad Pr_T = 1.0; \quad (3.19)$$

and the renormalization group model (Yakhot et al. 1992) gives

$$C_\mu = 0.0845, \quad Pr_T = 0.0719. \quad (3.20)$$

It can be found that although the values of C_μ given by both choices of the relaxation time are close to the classical $K - \epsilon$ model, the corresponding Prandtl numbers from the two choices exhibit significant differences. In particular, the choice of $\tau = K/(7\epsilon)$ produces a turbulent Prandtl

number of 0.7, which is quantitatively consistent with the well-established $K - \epsilon$ model parameters. In contrast, the case of $\tau = 6K/(7\epsilon)$ yields a Prandtl number of 4.2, which significantly exceeds the conventionally adopted range of $0.7 \sim 0.9$ in turbulence modelling (Kays 1994; Basu & Holtslag 2021). It is also noted that numerous studies choose $\text{Pr}_T = 1.0$ for simplicity, relying on the so-called Reynolds-analogy assumption (Tennekes & Lumley 1972; Sutton 2020).

Furthermore, a quantitative comparison is conducted between the Reynolds stress derived from the second-order CE expansion and the higher-order transport coefficients of some traditional quadratic nonlinear eddy viscosity models. When the nonlinear model is truncated to quadratic terms, σ can be expressed as

$$\sigma = -\frac{2K}{3}\mathbf{I} + 2C_\mu \frac{K^2}{\epsilon}\mathbf{S} - C_1 \frac{K^3}{\epsilon^2} \left[\mathbf{S} \cdot \mathbf{S} - \frac{1}{3}(\mathbf{S} : \mathbf{S})\mathbf{I} \right] - C_2 \frac{K^3}{\epsilon^2} (\mathbf{\Omega} \cdot \mathbf{S} - \mathbf{S} \cdot \mathbf{\Omega}) - C_3 \frac{K^3}{\epsilon^2} \left[\mathbf{\Omega} \cdot \mathbf{\Omega} - \frac{1}{3}(\mathbf{\Omega} : \mathbf{\Omega})\mathbf{I} \right], \quad (3.21)$$

where C_1 , C_2 and C_3 are three empirical coefficients in traditional nonlinear models. Table 1 lists the values for these coefficients in several typical quadratic nonlinear eddy viscosity models. The nonlinear terms derived directly from the second-order CE expansion exhibit quantitative agreement with those employed in nonlinear turbulence models. The present model incorporates additional terms that simultaneously account for both the material derivative of the strain tensor and higher-order TKE gradients, which are also considered in nonlinear turbulence models. It can be seen that the choice of $\tau = 6K/(7\epsilon)$ (Chen et al. 2023, 2024) gives higher-order transport coefficients that are larger than those of other nonlinear models, including the coefficients of the additional terms. In summary, the present kinetic model with $\tau = K/(7\epsilon)$ yields transport coefficients that are quantitatively close to those of established $K - \epsilon$ models and quadratic nonlinear eddy viscosity models, which have been obtained empirically or semi-empirically.

Model	C_μ	C_1	C_2	C_3	Additional terms
Speziale (1987)	0.09	-0.054	0	0	$-0.054 \frac{K^3}{\epsilon^2} (\dot{\mathbf{S}} - \frac{1}{3}(\text{tr}\dot{\mathbf{S}})\mathbf{I})$
Nisizima & Yoshizawa (1987)	0.09	-0.274	0.065	0.374	—
Rubinstein & Barton (1990)	0.0845	0.230	0.047	-0.190	—
Myong & Kasagi (1990b)	0.09	0.101	0.086	0.0178	$W_{\alpha\beta}$
Chen et al. (2023, 2024)	0.0816	0.280	0.140	0	$-\frac{0.14}{\epsilon} \frac{D}{Dt} [K^3 S/\epsilon] + \mathbf{Q}$
Present model	0.0816	0.047	0.023	0	$-\frac{-0.023}{\epsilon} \frac{D}{Dt} [K^3 S/\epsilon] + \mathbf{Q}$

$$\dot{\mathbf{S}} = \partial_t \mathbf{S} + (\mathbf{U} \cdot \nabla) \mathbf{S} - (\nabla \mathbf{U}) \mathbf{S} - \mathbf{S} (\nabla \mathbf{U})^T, \quad W_{\alpha\beta} = \frac{2}{3} \frac{\nu_0 K}{\epsilon} \left(\frac{\partial \sqrt{K}}{\partial x_\gamma} \right)^2 (-\delta_{\alpha\beta} - \delta_{\alpha\gamma}\delta_{\beta\gamma} + 4\delta_{\alpha\eta}\delta_{\beta\eta}),$$

$$\mathbf{Q} = -0.007 \frac{K}{\epsilon} \left[\nabla (K^2/\epsilon \nabla K) + (\nabla (K^2/\epsilon \nabla K))^T - \frac{2}{3} \nabla \cdot (K^2/\epsilon \nabla K) \mathbf{I} \right].$$

Table 1: Comparison of the transport coefficients with typical quadratic nonlinear eddy viscosity models.

4. Extension to wall-bounded turbulence

The kinetic turbulence model developed above is valid only for fully turbulent flows, which we refer to as the “high-Reynolds-number kinetic (HR-BGK) model”. However, in the near-wall region for wall-bounded flows, the turbulence is strongly damped and the effects of molecular viscosity become paramount (Hanjalić & Launder 1976). Furthermore, the turbulent motion is restricted and the relaxation time τ and the turbulent Reynolds number $Re_T = K^2/(\epsilon v_0)$ tend to zero. To address this challenge, a natural approach is to employ wall function methods from conventional turbulence modelling, which apply the HR-BGK model outside the viscous sublayer using empirical near-wall correlations. Alternatively, to enable resolution of flows within the viscous sublayer, we develop a low-Reynolds-number kinetic (LR-BGK) model that incorporates damping functions and an additional viscous diffusion term.

In the following subsections, we present the LR-BGK model, and the wall boundary conditions including non-slip condition for the LR-BGK model and wall function condition for the HR-BGK model.

4.1. Low-Reynolds-number kinetic model

In the near-wall region where the relaxation time τ is sufficiently small, the kinetic model asymptotically reduces to the linear eddy viscosity (3.8) and the gradient diffusion models (3.9). Most contemporary low Reynolds number $K - \epsilon$ models retain the transport-equation structure first introduced by Jones & Launder (1972); they differ mainly in the addition of (i) van Driest damping function f_μ , which is small within the near-wall region, and tends to unity in bulk region, and (ii) explicit molecular diffusion term $v_0 \nabla^2 K$ of which are essential to represent the strong viscous diffusion of TKE that dominates within the viscous near-wall region.

First, to incorporate the van Driest damping function f_μ explicitly into the turbulent viscosity formulation, the relaxation time τ is redefined as,

$$\tau = \frac{f_\tau}{7} \frac{K}{\epsilon}, \quad (4.1)$$

where f_τ is a damping function corresponding to f_μ . To match the turbulent viscosity definition in (3.9) with the classical expression incorporating the van Driest damping function f_μ , we equate:

$$\nu_T = \frac{2\tau K^{eq}}{3} = C_\mu f_\mu \frac{K^2}{\epsilon}, \quad C_\mu = 0.0816. \quad (4.2)$$

Then with the relationship $K^{eq} = K - \tau \epsilon$ and the expression (4.1), we can obtain

$$\frac{2f_\tau (1 - f_\tau/7)}{21} = C_\mu f_\mu, \quad (4.3)$$

which gives

$$f_\tau = \frac{7 - \sqrt{49 - 24f_\mu}}{2}. \quad (4.4)$$

Note that here the physical constraint $0 \leq f_\tau \leq 1$ is considered to ensure physically meaningful values. A number of damping functions have been proposed. For instance, the expression proposed by Jones & Launder (1972) depends solely on Re_T . Subsequent refinements by Myong & Kasagi (1990a) and Nagano & Tagawa (1990) introduce dependencies on the dimensionless wall coordinate (y^+), thus explicitly incorporating sensitivity to near-wall length scales into the turbulence model.

Secondly, the explicit molecular viscosity diffusion $v_0 \nabla^2 K$ is incorporated by introducing an additional source term \mathcal{S} into the kinetic equation

$$\partial_t F + \boldsymbol{\xi} \cdot \nabla F + \bar{\boldsymbol{a}} \cdot \nabla_{\boldsymbol{\xi}} F = C(F) + \mathcal{S}, \quad (4.5)$$

where \mathcal{S} satisfies the following moment requirements,

$$\int \mathcal{S} d\xi = 0, \quad \int \xi \mathcal{S} d\xi = 0, \quad \frac{1}{2} \int (\xi - \mathbf{U})^2 \mathcal{S} d\xi = \nu_0 \nabla^2 K. \quad (4.6)$$

There are many possible ways to design the specific form of the source term. Analogous to the formulation proposed by [Lundgren \(1969\)](#) for the dissipation term, we can choose

$$\mathcal{S} = -\frac{\nu_0 \nabla^2 K}{2K^{eq}} \nabla_\xi \cdot [(\xi - \mathbf{U}) F]. \quad (4.7)$$

Alternatively, following the well-known Shakhov model ([Shakhov 1968](#)) for non-equilibrium rarefied gas flows and applying the Hermite-polynomial expansion method, we can obtain an alternative formulation,

$$\mathcal{S} = \frac{3\nu_0 \nabla^2 K}{2K^{eq}} \left(\frac{(\xi - \mathbf{U})^2}{2K^{eq}} - 1 \right) F^{eq}. \quad (4.8)$$

Note that the above construction is formally equivalent to replacing F with its equilibrium counterpart F^{eq} in (4.7). This approximation is justified, because the viscous diffusion of TKE is relevant only when the turbulent Reynolds number Re_T (and therefore the relaxation time τ) is small, a regime in which the VDF remains close to equilibrium.

4.2. Wall boundary conditions

A central challenge in applying kinetic theory to turbulence is the formulation of physically consistent boundary conditions because there is no experimentally or theoretically established expression for the VDF at a solid wall. In analogy with conventional turbulence models, the wall distribution function $F(\mathbf{x}_w)$ is required to satisfy the following moment constraints:

$$\begin{aligned} \int \xi F(\mathbf{x}_w) d\xi &= \mathbf{U}_w, \\ \frac{1}{2} \int (\xi - \mathbf{U}(\mathbf{x}_w))^2 F(\mathbf{x}_w) d\xi &= K_w, \end{aligned} \quad (4.9)$$

where \mathbf{x}_w denotes a point on the wall interface. The prescribed wall velocity \mathbf{U}_w and turbulent kinetic energy K_w are assigned according to the turbulence model: for LR-BGK model, they reduce to strict non-slip velocity and zero TKE, whereas for HR-BGK model, they are supplied by empirical wall functions ([Lauder & Spalding 1983](#)), namely the logarithmic law for velocity and the corresponding estimation of TKE.

However, different choices of F can satisfy the integral constraints in (4.9), so that $F(\mathbf{x}_w)$ itself is not unique. A similar situation is encountered in rarefied gas from the kinetic theory, where the establishment of accurate solutions has led to a dedicated research field focused on modelling gas–surface interactions for boundary conditions ([Cercignani & Lampis 1971; Cercignani 1972; Lord 1991; Aoki et al. 2022; Kosuge et al. 2025](#)). An equally specialized effort will likely be required to develop reliable wall boundary conditions in kinetic representation of the average turbulence dynamics. Here, by leveraging boundary conditions from kinetic theory, we generalize two well-known boundary conditions of rarefied gas, namely the fully diffuse Maxwell boundary condition ([Maxwell 1879](#)) and the non-equilibrium extrapolation boundary condition ([Guo et al. 2002](#)), to turbulent flows.

The fully diffuse Maxwell boundary condition ([Maxwell 1879](#)) is employed in the LR-BGK model to enforce the non-slip velocity and the zero TKE at the wall. Importantly, this boundary condition produces a velocity slip and a TKE jump that both diminish linearly as τ decreases. In the near-wall region, τ is sufficiently small, so the induced slip and TKE jump are negligible, and the classical non-slip and zero-TKE limits are effectively recovered. In this boundary condition,

it is assumed that particles leaving the surface follow an equilibrium VDF with the wall velocity and TKE,

$$F(\mathbf{x}_w, \boldsymbol{\xi}) = \alpha_w F^{eq}(\boldsymbol{\xi}; \mathbf{U}_w, K_w), \quad \boldsymbol{\xi} \cdot \mathbf{n}_w > 0, \quad (4.10)$$

where \mathbf{n}_w is the unit vector normal to the wall pointing to the cell, and α_w is the coefficient at the wall determined by the condition of zero mass flux,

$$\int_{\boldsymbol{\xi} \cdot \mathbf{n}_w \leq 0} (\boldsymbol{\xi} \cdot \mathbf{n}_w) F(\mathbf{x}_w, \boldsymbol{\xi}) d\boldsymbol{\xi} + \int_{\boldsymbol{\xi} \cdot \mathbf{n}_w > 0} (\boldsymbol{\xi} \cdot \mathbf{n}_w) \alpha_w F^{eq}(\boldsymbol{\xi}; \mathbf{U}_w, K_w) d\boldsymbol{\xi} = 0, \quad (4.11)$$

which gives

$$\alpha_w = - \frac{\int_{\boldsymbol{\xi} \cdot \mathbf{n}_w \leq 0} (\boldsymbol{\xi} \cdot \mathbf{n}_w) F(\mathbf{x}_w, \boldsymbol{\xi}) d\boldsymbol{\xi}}{\int_{\boldsymbol{\xi} \cdot \mathbf{n}_w > 0} (\boldsymbol{\xi} \cdot \mathbf{n}_w) F^{eq}(\boldsymbol{\xi}; \mathbf{U}_w, K_w) d\boldsymbol{\xi}}. \quad (4.12)$$

In practice, K_w is set to a very small positive value rather than exactly zero for numerical stability.

On the other hand, for the HR-BGK model that is applicable outside the viscous sublayer, the non-equilibrium extrapolation boundary condition (Guo et al. 2002) in conjunction with an empirical wall function (Lauder & Spalding 1983) is adopted. In the near-wall region, the mean velocity follows the classical logarithmic law, and the wall function is applied only inside the log-layer ($15 \lesssim y^+ \lesssim 200$), bypassing the viscous sublayer:

$$\frac{U(y)}{U_\sigma} = \frac{1}{\kappa} \ln(y^+) + B, \quad (4.13)$$

where $U_\sigma = \sqrt{\sigma_w}$ is the friction velocity obtained from the wall shear stress σ_w with unity density, $\kappa \approx 0.41$ is the von Kármán constant, and B is an empirical constant related to the thickness of the viscous sublayer; y denotes the wall-normal distance measured from the wall into the fluid and $y^+ = U_\sigma y / \nu_0$ is its dimensionless form. The corresponding wall value of the TKE is specified by the usual log-layer estimate,

$$K_w = U_\tau^2 / \sqrt{C_\mu}. \quad (4.14)$$

The VDF reflected from the wall located at the interface \mathbf{x}_w is then reconstructed by the non-equilibrium extrapolation boundary condition (Guo et al. 2002),

$$F(\mathbf{x}_w, \boldsymbol{\xi}) = F^{eq}(\boldsymbol{\xi}; \mathbf{U}_w, K_w) - [F(\mathbf{x}_{nc}, \boldsymbol{\xi}) - F^{eq}(\mathbf{x}_{nc}; \mathbf{U}(\mathbf{x}_{nc}), K(\mathbf{x}_{nc}))], \quad \boldsymbol{\xi} \cdot \mathbf{n}_w > 0, \quad (4.15)$$

where \mathbf{x}_{nc} is the neighboring cell of \mathbf{x}_w . The equilibrium term enforces the prescribed wall function moments, while the second term extrapolates the non-equilibrium part of the VDF, ensuring compatibility with the interior solution. It is worth noting that the non-equilibrium extrapolation method assumes that the deviation from equilibrium is small to permit linear extrapolation. For highly non-equilibrium turbulent flows, this method may fail to work properly.

5. Study of turbulent plane Couette flow

The turbulent plane Couette flow provides an ideal benchmark (Henry & Reynolds 1984; Nisizima & Yoshizawa 1987; Schneider 1989; Andersson & Pettersson 1994) to test whether the present kinetic model can accurately capture wall-bounded shear turbulence. The LR-BGK and HR-BGK models, coupled with the diffuse and non-equilibrium extrapolation boundary conditions, respectively, are employed to simulate this flow at different Reynolds numbers. The central issue in wall-bounded shear turbulence is the prediction of mean velocity profiles and the derivation of friction laws. In this study, we consider the configuration of steady turbulent Couette flow between two infinite parallel plates located at $y = \pm h$, as illustrated in figure 1. The two plates move in opposite directions with constant velocities $\pm U_w$ in the x -direction, respectively. The corresponding Reynolds number is defined as $\text{Re} = U_w h / \nu_0$.

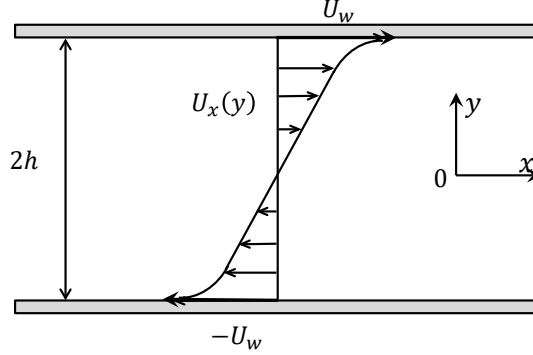


Figure 1: Sketch of turbulent plane Couette flow between two infinite parallel plates separated by $2h$. The plates move in opposite directions with constant velocities $\pm U_w$ in the x -direction, generating a monotonic mean velocity profile $U_x(y)$.

5.1. Numerical method and parameter set-up

As mentioned in §2.2, the dissipation rate ϵ is an input parameter to determine the relaxation time τ in the present kinetic model. For the HR-BGK model, we adopt the widely used transport equation for the dissipation rate ϵ proposed by [Launder & Spalding \(1983\)](#) to calculate ϵ ,

$$\frac{\partial \epsilon}{\partial t} + (\mathbf{U} \cdot \nabla) \epsilon = \nabla \cdot \left(\frac{\nu_T}{C_\epsilon} \nabla \epsilon \right) + C_{\epsilon 1} \frac{\epsilon}{K} \boldsymbol{\sigma} : \nabla \mathbf{U} - C_{\epsilon 2} \frac{\epsilon^2}{K}, \quad (5.1)$$

where $\nu_T = 0.09K^2/\epsilon$, $C_\epsilon = 1.3$, $C_{\epsilon 1} = 1.44$ and $C_{\epsilon 2} = 1.92$. It is worth highlighting that both the turbulent kinetic energy K and the stress tensor $\boldsymbol{\sigma}$ are obtained directly from the solution of kinetic equation; therefore, equation (5.1) retains higher-order non-equilibrium information that is absent from the linear eddy viscosity model. The corresponding wall boundary condition for the Couette flow employs a wall function approach, where the wall value of ϵ is specified according to the usual logarithmic layer estimate,

$$\epsilon_w = \frac{U_\sigma^3}{\kappa y_1}, \quad (5.2)$$

with y_1 being the wall-normal distance from the wall to the center of the first grid cell adjacent to the wall.

On the other hand, for the LR-BGK model, an alternative transport equation for ϵ with wall damping effect ([Nagano & Tagawa 1990](#)) is adopted,

$$\frac{\partial \epsilon}{\partial t} + (\mathbf{U} \cdot \nabla) \epsilon = \nabla \cdot \left(\frac{\nu_T}{C_\epsilon} \nabla \epsilon \right) + C_{\epsilon 1} \frac{\epsilon}{K} \boldsymbol{\sigma} : \nabla \mathbf{U} - C_{\epsilon 2} f_{\epsilon 2} \frac{\epsilon^2}{K}, \quad (5.3)$$

where $\nu_T = 0.09 f_\mu K^2/\epsilon$, $C_\epsilon = 1.3$, $C_{\epsilon 1} = 1.45$ and $C_{\epsilon 2} = 1.92$. f_μ and $f_{\epsilon 2}$ are the damping functions, defined as

$$f_\mu = \left(1 - \exp \left(-\frac{-y^+}{26} \right) \right)^2 \left(1 + \frac{4.1}{\text{Re}_T^{3/4}} \right),$$

$$f_{\epsilon 2} = \left(1 - 0.3 \exp \left(-\frac{\text{Re}_T^2}{42.5} \right) \right) \left(1 - \exp \left(-\frac{-y^+}{6} \right) \right)^2. \quad (5.4)$$

The corresponding wall boundary condition is

$$\epsilon_w = \nu_0 \left(\frac{\partial \sqrt{K}}{\partial y} \right)^2. \quad (5.5)$$

Since the turbulent Couette flow is a quasi-one-dimensional problem, the computational cost can be reduced by introducing the following reduced distribution functions,

$$(\Phi_1, \Phi_2, \Phi_3, \Phi_4)^T = \int \left(1, \xi_x, \xi_x^2, \xi_z^2 \right)^T F(\mathbf{x}, \xi, t) d\xi_x d\xi_z. \quad (5.6)$$

These reduced VDFs carry distinct essential physics in the context of turbulent transport. Φ_1 represents the local mass density distribution in velocity space, directly related to the continuity equation and mass conservation. Φ_2 corresponds to the streamwise momentum distribution, governing the transport of momentum in the flow direction and thus controlling the Reynolds shear stress generation. Φ_3 characterizes the streamwise TKE distribution, which is crucial for understanding the anisotropic energy transport and the development of velocity fluctuations (or Reynolds normal stress). Finally, Φ_4 represents the vertical kinetic energy distribution, capturing the cross-flow energy transport mechanisms. Together, these reduced VDFs encapsulate the essential physics of momentum and energy transport in wall-bounded turbulent flows while significantly reducing the computational complexity compared to the full three-dimensional kinetic equation.

The reduced kinetic equations for the four Φ_k 's are then solved using a discretized velocity method; further details can be found in Appendix B. To ensure accurate approximation of macroscopic moments in velocity space across various Re , computational parameters, including the spatial mesh size and the discretization of velocity space, must be carefully selected through convergence studies until solution variations become negligible.

In our simulations, the computational domain is set to be $[-h, h]$. For the HR-BGK model, the computational domain is uniformly discretized, with the cell size determined according to different Re . The selection criterion ensures that the first cell center point is located inside the logarithmic layer. For the LR-BGK model, the nonuniform meshes are adopted to improve the prediction by using a locally refine mesh close to the boundary. The mesh points are given by $y_j/(2h) = (\zeta_j + \zeta_{j+1})/2$ for $0 \leq j \leq N_y - 1$, where ζ_j is defined by

$$\zeta_j = \frac{\tanh(a(j/N_y - 1/2))}{2 \tanh(a/2)}, \quad j = 0, 1, \dots, N_y, \quad (5.7)$$

with a being a dimensionless stretching parameter controlling the characteristics of the mesh distribution, and N_y is the number of mesh cells. In the present study, a is taken as 2.5. We utilize $N_y = 401$ cells for the LR-BGK model, ensuring that the center of the first off-wall cell lies within the viscous sublayer for all cases considered. The velocity space truncated at $[-5\sqrt{U_w}, 5\sqrt{U_w}]$ is discretized by the trapezoidal rule (Wu et al. 2014) with 4000 non-uniform velocity grid points. Furthermore, the time step is set to $0.05 \times 5\sqrt{U_w}/(\Delta y_{min})$ with y_{min} being the minimum cell size. The steady-state solution is considered to be achieved when the maximum relative change in the velocity field between two consecutive iterations falls below 10^{-10} .

5.2. Comparison with experiments and direct numerical simulations

The present kinetic model is validated by comparing the predictions against benchmark data from experiments and DNS solutions. The comparison focuses on key flow parameters including mean velocity profiles, dimensionless velocity distributions, skin friction coefficients, and Reynolds stress components.

The mean velocity profiles predicted by the LR-BGK and HR-BGK models are compared with

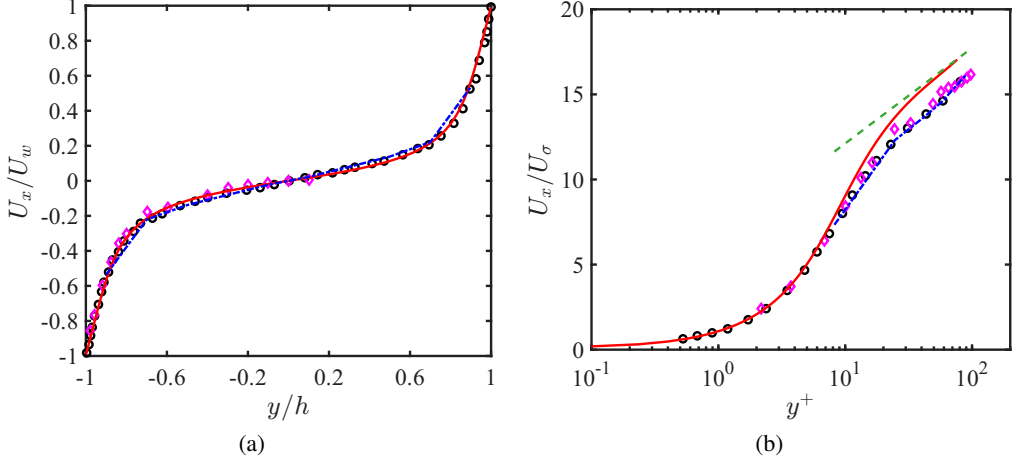


Figure 2: Mean velocity profiles scaled in (a) outer and (b) wall units of the turbulent Couette flow. The solid and dash-dot lines represent the predictions of the LR-BGK model and the HR-BGK model at $Re = 1300$, respectively. The diamonds denote the experimental data of [Bech et al. \(1995\)](#) at $Re = 1260$, and the circles denote the DNS data of [Bech et al. \(1995\)](#) at $Re = 1300$. The dashed line represents the classical logarithmic law profile $(\ln y^+)/0.41 + 6.5$.

the experimental ([Bech et al. 1995](#); [Robertson 1959b](#)) and DNS ([Bech et al. 1995](#); [Pirozzoli et al. 2014](#)) data at $Re = 1300$ and 10133 , as shown in figures 2 and 3. The results are presented in both outer units (scaled by U_w and h) and wall units (scaled by U_σ and y^+) to examine the performance of the models across different flow regions. In the case of $Re = 1300$, Figure 2a demonstrates that both models accurately capture the overall velocity distribution in outer coordinates, closely matching the experimental and DNS data of [Bech et al. \(1995\)](#). Specifically, the LR-BGK model shows excellent agreement throughout the entire flow domain, while the HR-BGK model exhibits slightly larger deviations in the near-wall region, which can be expected since the viscous sublayer is bypassed in the wall function boundary condition. At a higher Reynolds number ($Re = 10133$), figure 3 shows that both the HR-BGK and LR-BGK models maintain their predictive accuracy, in good agreement with the experimental data of [Robertson \(1959b\)](#) and DNS data of [Pirozzoli et al. \(2014\)](#), though both models exhibit slightly larger deviations in the near-wall region. The logarithmic law profile (4.13) is well-captured by both models with $\kappa = 0.41$, using $B = 6.5$ and 7.0 for $Re = 1300$ and 10133 , respectively.

Figure 4 presents the variation of the skin friction coefficient C_f with Reynolds number, together with the comparisons with extensive experimental ([Kitoh et al. 2005](#); [El Telbany & Reynolds 1980](#); [Reichardt 1956](#); [Robertson 1959a](#)) and DNS ([Bech et al. 1995](#); [Tsukahara et al. 2006](#); [Pirozzoli et al. 2014](#)) databases. The friction coefficient is defined as

$$C_f = \frac{\sigma_w}{\frac{1}{2}U_w^2}, \quad (5.8)$$

where σ_w is the wall shear stress obtained directly from the VDFs. Both models demonstrate excellent agreement with the experimental data for Re between 10^3 to 10^4 . The LR-BGK model shows minor deviations in the lower Re range, with deviations typically less than 5% from the data of [Kitoh et al. \(2005\)](#); [Bech et al. \(1995\)](#); [Tsukahara et al. \(2006\)](#). The HR-BGK model maintains consistent accuracy across the entire Re range, showing good agreement with both experimental and DNS data.

The Reynolds shear stress profiles provide a stringent test of the capacity of the models

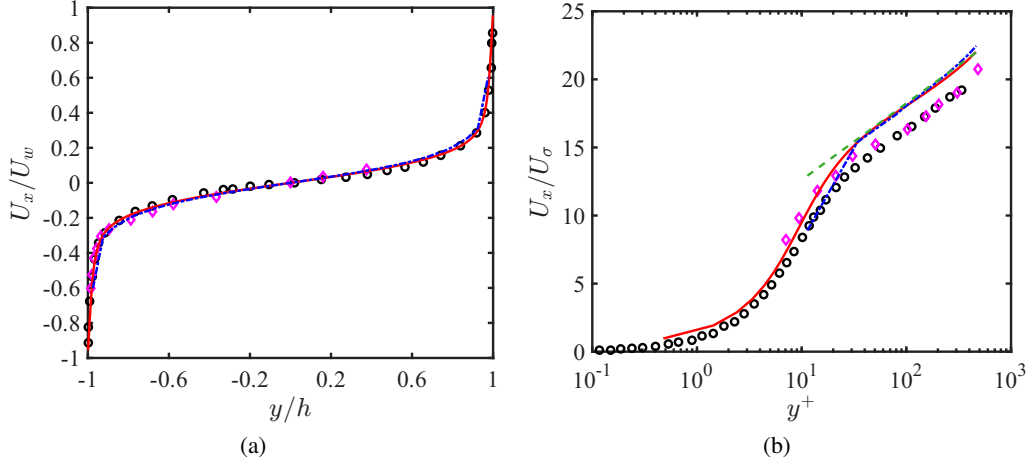


Figure 3: Mean velocity profiles scaled in (a) outer and (b) wall units of turbulent Couette flow. The solid and dash-dot lines represent the predictions of the LR-BGK model and the HR-BGK model at $Re = 10133$, respectively. The diamonds denote the experimental data of [Robertson \(1959b\)](#) at $Re = 10000$, and the circles denote the DNS data of [Pirozzoli et al. \(2014\)](#) at $Re = 10133$. The dashed line represents the classical logarithmic law profile $(\ln y^+) / 0.41 + 7$.

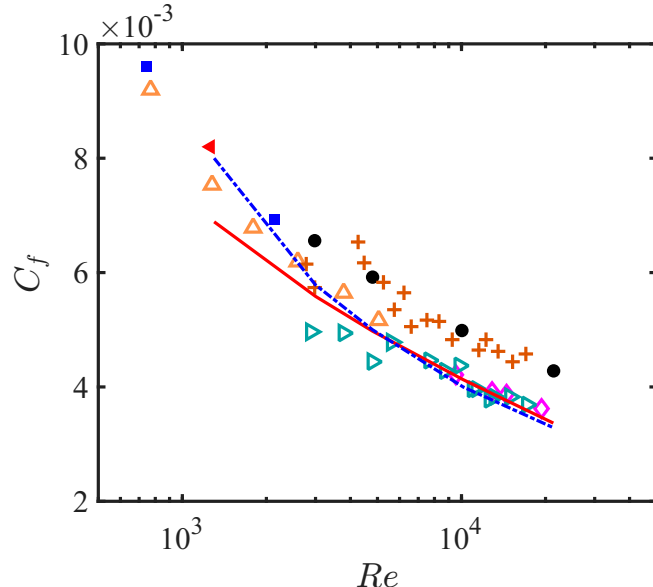


Figure 4: Variation of skin friction coefficient with Reynolds number. The solid and dash-dot lines represent the predictions of the LR-BGK model and the HR-BGK model, respectively. Open symbols refer to experimental data by [Kitoh et al. \(2005\)](#) (triangles), [El Telbany & Reynolds \(1980\)](#) (diamonds), [Reichardt \(1956\)](#) (right-pointing triangles), [Robertson \(1959a\)](#) (pluses). Filled symbols refer to DNS data by [Bech et al. \(1995\)](#) (left-pointing triangles), [Tsukahara et al. \(2006\)](#) (squares), [Pirozzoli et al. \(2014\)](#) (circles).

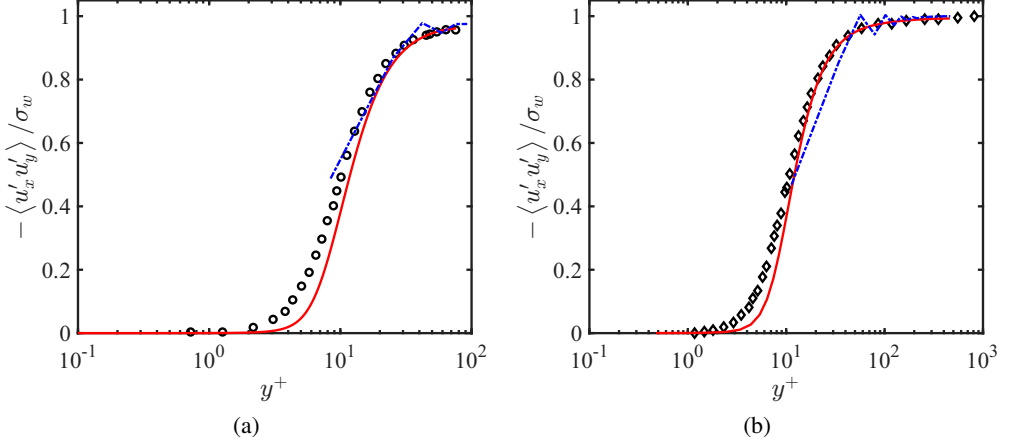


Figure 5: Reynolds shear stress profiles scaled in wall units of turbulent Couette flow at (a) $Re = 1300$ and (b) $Re = 10133$. The solid and dash-dot lines represent the predictions of the LR-BGK model and the HR-BGK model, respectively. The circles and the diamonds denote the DNS data of [Bech et al. \(1995\)](#) and [Pirozzoli et al. \(2014\)](#), respectively.

to capture turbulent momentum transport mechanisms. Figure 5 compares the dimensionless Reynolds shear stress $-\langle u'_x u'_y \rangle / \sigma_w$ predicted by both kinetic models with DNS data ([Bech et al. 1995](#); [Pirozzoli et al. 2014](#)) as Re ranges from 1300 to 10133. It is noteworthy that the HR-BGK model, due to its coarser grid resolution, exhibits minor numerical oscillations in the near-wall region. Both kinetic models exhibit excellent agreement with the DNS data, accurately capturing both the peak value and its location, particularly in the logarithmic and outer regions ($y^+ \geq 15$). However, the LR-BGK model shows some deviations in the transition region ($1 < y^+ < 15$) due to the inherent complexity of this region where viscous and turbulent effects compete.

Figures 6 and 7 present detailed comparisons of the velocity fluctuation intensities (normal Reynolds stress) in all three spatial directions which can provide insight into the anisotropic nature of near-wall turbulence, which the linear eddy viscosity model (3.8) cannot capture ([Lauder & Sharma 1974](#)). The velocity fluctuation intensities predicted by the present models show noticeable differences from the DNS data ([Bech et al. 1995](#); [Pirozzoli et al. 2014](#)), with the discrepancies becoming more pronounced at higher Re . At $Re = 1300$, the dimensionless streamwise $\sqrt{\langle (u'_x)^2 \rangle}$ and vertical $\sqrt{\langle (u'_z)^2 \rangle}$ components exhibit relatively small deviations from DNS data near the channel centerline, while the differences become increasingly evident as Re increases to 10133. The LR-BGK model demonstrates superior performance in capturing the peak locations of the streamwise fluctuations, where the peak occurs around $y^+ \approx 10$. Although the present models do not provide a clear separation between the normal stress components, they demonstrate the capability to capture non-Newtonian effects (nonlinear eddy viscosity effects) as mentioned in §3. This non-equilibrium phenomenon, often reported in rarefied gas flows at finite Knudsen numbers, exhibits the anisotropic stress behaviour that cannot be captured by the NS equations ([Xu et al. 2007](#)).

5.3. Non-equilibrium characteristics and velocity distribution functions

The non-equilibrium and non-Newtonian characteristics predicted by the present kinetic model can be essentially explained from the VDFs. We now examine the reduced VDFs obtained from both the LR-BGK and HR-BGK models at $Re = 10133$, comparing the computed VDFs with

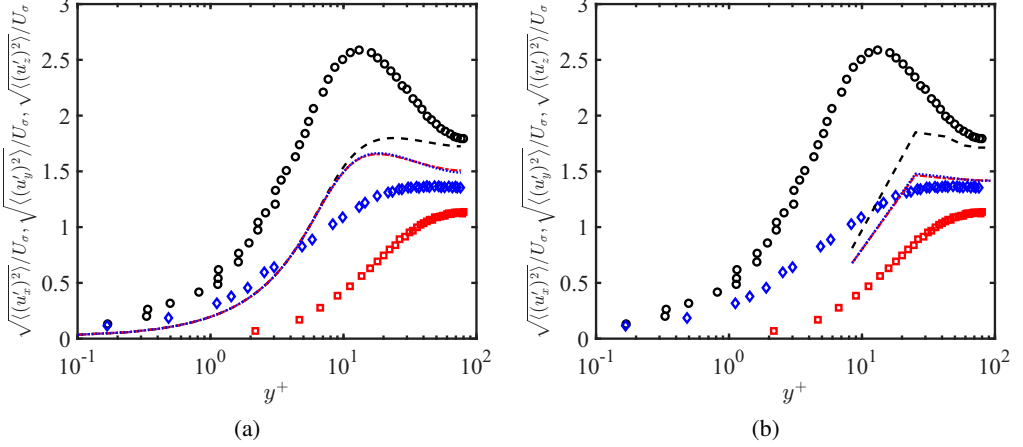


Figure 6: Distribution of the velocity fluctuation intensities (Reynolds normal stress) scaled in wall units of turbulent Couette flow from (a) the LR-BGK model and (b) the HR-BGK model at $\text{Re} = 1300$. The dash, dash-dot and dot lines represent $\sqrt{\langle (u'_x)^2 \rangle}/U_\sigma$, $\sqrt{\langle (u'_y)^2 \rangle}/U_\sigma$ and $\sqrt{\langle (u'_z)^2 \rangle}/U_\sigma$, respectively. The symbols denote the DNS data of [Bech et al. \(1995\)](#): $\sqrt{\langle (u'_x)^2 \rangle}/U_\sigma$ (circles), $\sqrt{\langle (u'_y)^2 \rangle}/U_\sigma$ (squares) and $\sqrt{\langle (u'_z)^2 \rangle}/U_\sigma$ (diamonds).

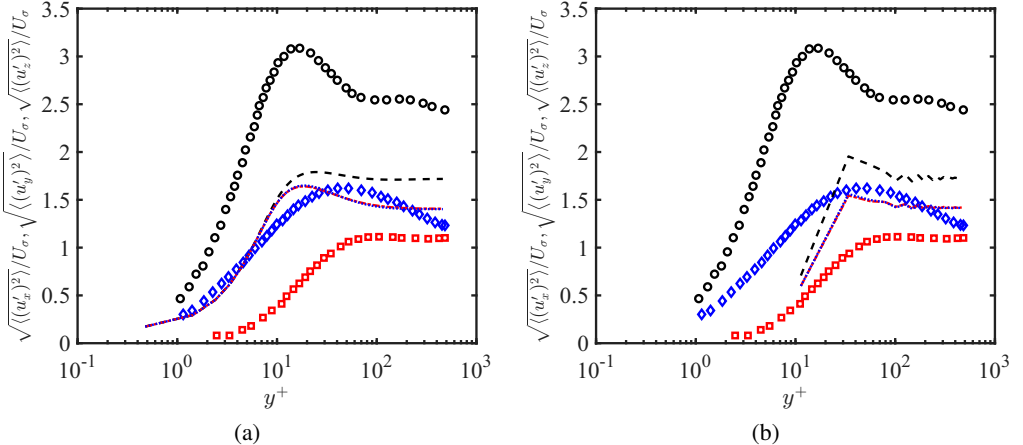


Figure 7: Distribution of the velocity fluctuation intensities (Reynolds normal stress) scaled in wall units of turbulent Couette flow from (a) the LR-BGK model and (b) the HR-BGK model at $\text{Re} = 10133$. The dash, dash-dot and dot lines represent $\sqrt{\langle (u'_x)^2 \rangle}/U_\sigma$, $\sqrt{\langle (u'_y)^2 \rangle}/U_\sigma$ and $\sqrt{\langle (u'_z)^2 \rangle}/U_\sigma$, respectively. The symbols denote the DNS data of [Pirozzoli et al. \(2014\)](#): $\sqrt{\langle (u'_x)^2 \rangle}/U_\sigma$ (circles), $\sqrt{\langle (u'_y)^2 \rangle}/U_\sigma$ (squares) and $\sqrt{\langle (u'_z)^2 \rangle}/U_\sigma$ (diamonds).

their corresponding local equilibrium distributions to quantify the degree of departure from equilibrium.

Figures 8 and 9 present the reduced velocity distribution functions Φ_1 , Φ_2 , and Φ_3 as functions of microscopic velocity ξ_y in various normal wall positions ranging from the viscous sublayer to the centerline of the channel, compared against the local equilibrium VDFs derived from the local mean velocity and turbulent kinetic energy. Here ξ_y in the region $[-3\xi_m, 3\xi_m]$ with $\xi_m = \sqrt{4K/3}$ represents the most probable velocity scale based on the local turbulent kinetic energy. The fourth VDF Φ_4 , which exhibits behaviour similar to Φ_1 by remaining close to equilibrium, is presented in Appendix C.

The most striking observation is the markedly different behaviours exhibited by the various reduced VDFs. The distribution function Φ_1 , which represents the zeroth-order moment in the wall-normal direction, remains remarkably close to its local equilibrium state across all wall-normal positions and for both kinetic models. This near-equilibrium behaviour indicates that the mass conservation constraint is well satisfied throughout the flow domain, consistent with the incompressibility condition. In sharp contrast, Φ_2 and Φ_3 exhibit pronounced departures from their respective equilibrium distributions, particularly in the outer region of the flow. The VDF Φ_2 , associated with the streamwise momentum transport, shows increasing non-equilibrium effects as the distance from the wall increases. Notably, at $y^+ \approx 419$ and the channel centerline, Φ_2 exhibits distinctly non-Gaussian distributions, indicating the presence of intermittent large-scale turbulent structures that cannot be captured by simple equilibrium assumptions. Similarly, Φ_3 , which is related to the streamwise kinetic energy transport, demonstrates substantial non-equilibrium characteristics with a comparable spatial evolution pattern. The VDF Φ_3 shows progressively stronger departures from equilibrium as the wall-normal distance increases, with the outer region exhibiting the most pronounced non-equilibrium effects. Remarkably, Φ_3 also displays non-Gaussian distributions at $y^+ \approx 419$ and the channel centerline. The non-equilibrium nature of Φ_3 directly contributes to the anisotropic stress behaviour observed in the Reynolds stress predictions, explaining the model's capability to capture the non-Newtonian effects that linear eddy viscosity models cannot represent.

The comparison between the LR-BGK and HR-BGK models reveals consistent non-equilibrium patterns, with the LR-BGK model providing slightly more detailed resolution of the near-wall non-equilibrium effects due to its finer grid resolution in the viscous sublayer. Overall, both kinetic models successfully capture the essential physics of the non-equilibrium turbulent transport processes, demonstrating the robustness of the kinetic approach across different near-wall treatments and grid resolutions. To further quantify the degree of departure from equilibrium, we examine the second-order moment of $F - F^{eq}$

$$\sigma^{neq} = - \int (\xi - \mathbf{U}) (\xi - \mathbf{U}) (F - F^{eq}) d\xi. \quad (5.9)$$

It should be noted that the zeroth and first-order moments of $F - F^{eq}$ vanish identically. In the case of plane Couette flow, equation (3.12) reduces to:

$$\begin{aligned} \sigma_{xy}^{CE} &= \nu_T \frac{\partial U_x}{\partial y}, \\ \sigma_{xx}^{CE} &= -\frac{2}{3} K - \frac{2\nu_T^2}{K^{eq}} \left(\frac{\partial U_x}{\partial y} \right)^2 + \frac{2\nu_T}{3K^{eq}} \frac{\partial}{\partial y} \left(\nu_T \frac{\partial K^{eq}}{\partial y} \right), \\ \sigma_{yy}^{CE} &= -\frac{2}{3} K + \frac{\nu_T^2}{K^{eq}} \left(\frac{\partial U_x}{\partial y} \right)^2 - \frac{4\nu_T}{3K^{eq}} \frac{\partial}{\partial y} \left(\nu_T \frac{\partial K^{eq}}{\partial y} \right), \\ \sigma_{zz}^{CE} &= -\frac{2}{3} K + \frac{\nu_T^2}{K^{eq}} \left(\frac{\partial U_x}{\partial y} \right)^2 + \frac{2\nu_T}{3K^{eq}} \frac{\partial}{\partial y} \left(\nu_T \frac{\partial K^{eq}}{\partial y} \right), \end{aligned} \quad (5.10)$$

where $\nu_T = 0.0816 f_\mu K^2 / \epsilon$. These expressions indicate significant differences among the three normal stress components, demonstrating the capability of the present kinetic model to capture anisotropic stress behaviour.

Figures 10 and 11 present the deviatoric part of σ^{neq} predicted by LR-BGK model at $Re = 10133$ and compare them with the CE expansion results given by equation (3.12). It can be seen that the deviatoric Reynolds stress shows good agreement between the LR-BGK model and the CE expansion throughout the flow domain, validating the theoretical consistency of the kinetic approach. The minor discrepancies observed can be attributed to higher-order terms in the CE expansion that are not captured by the second-order analysis. Furthermore, the deviatoric Reynolds normal stress components better reflect the degree of departure from non-equilibrium of the VDFs mentioned above. In the viscous sublayer and buffer region, the system remains essentially in equilibrium with all three normal stress components close to zero, while in the outer layer non-equilibrium effects become more pronounced as the deviations from zero increase progressively.

These non-equilibrium characteristics, as revealed through both the VDFs and their non-equilibrium moments, provide a fundamental explanation for the superior performance of the kinetic models in capturing the anisotropic Reynolds stress behaviour and the associated non-Newtonian effects. The departure from local equilibrium enables the kinetic approach to naturally account for the complex momentum and energy transport mechanisms that arise from the finite relaxation times of turbulent eddies, analogous to the finite collision times in rarefied gas flows. This non-equilibrium characteristic is particularly important in wall-bounded flows, where the presence of the wall creates strong gradients and anisotropic conditions that drive the system away from local Gaussian equilibrium.

6. Conclusions

In this work, we extended and analyzed the kinetic model for incompressible turbulence proposed by [Chen et al. \(2023\)](#) and demonstrated improved applicability and physical consistency. By redefining the relaxation time as $\tau = K/(7\epsilon)$, the Chapman–Enskog expansion of the kinetic model yielded linear and nonlinear eddy viscosity and gradient diffusion closures with transport coefficients ($C_\mu = 0.0816$, $Pr_T = 0.7$) that are in quantitative agreement with those of conventional turbulence models. The analysis of our kinetic model reveals that its second-order expansion generates various material derivatives and higher-order derivatives of TKE. Unlike previous results for the Boltzmann–BGK equation without TKE dissipation ([Chen et al. 2004](#)) or for the Fokker–Planck equation ([Heinz 2007](#); [Luan et al. 2025](#)), the analysis of our kinetic model yielded different forms of material derivatives for the linear terms and higher-order derivative terms involving TKE from the second-order expansion. To our knowledge, such closed-form Chapman–Enskog expressions for the TKE flux and its nonlinear corrections have not previously been reported for this class of turbulent kinetic models.

To address wall-bounded turbulence, we developed two approaches within a unified kinetic framework. For applications outside the viscous sublayer, the non-equilibrium extrapolation boundary condition based on wall function approaches was proposed for the HR-BGK model, maintaining accurate logarithmic layer behaviour at lower computational expense. For direct viscous sublayer resolution, we constructed a low-Reynolds-number kinetic model incorporating a damping function and a viscous diffusion term, with the fully diffuse wall condition. It is worth noting that the present methods for wall-bounded flows are fundamentally different from the boundary conditions based on the wall function method of [Srinivasan et al. \(1977\)](#), devised for the kinetic model of [Lundgren \(1969\)](#). Our approach is not restricted to regions outside the viscous sublayer, enabling treatment of the complete flow domain from wall to bulk region.

The present kinetic models were comprehensively validated against experimental data and

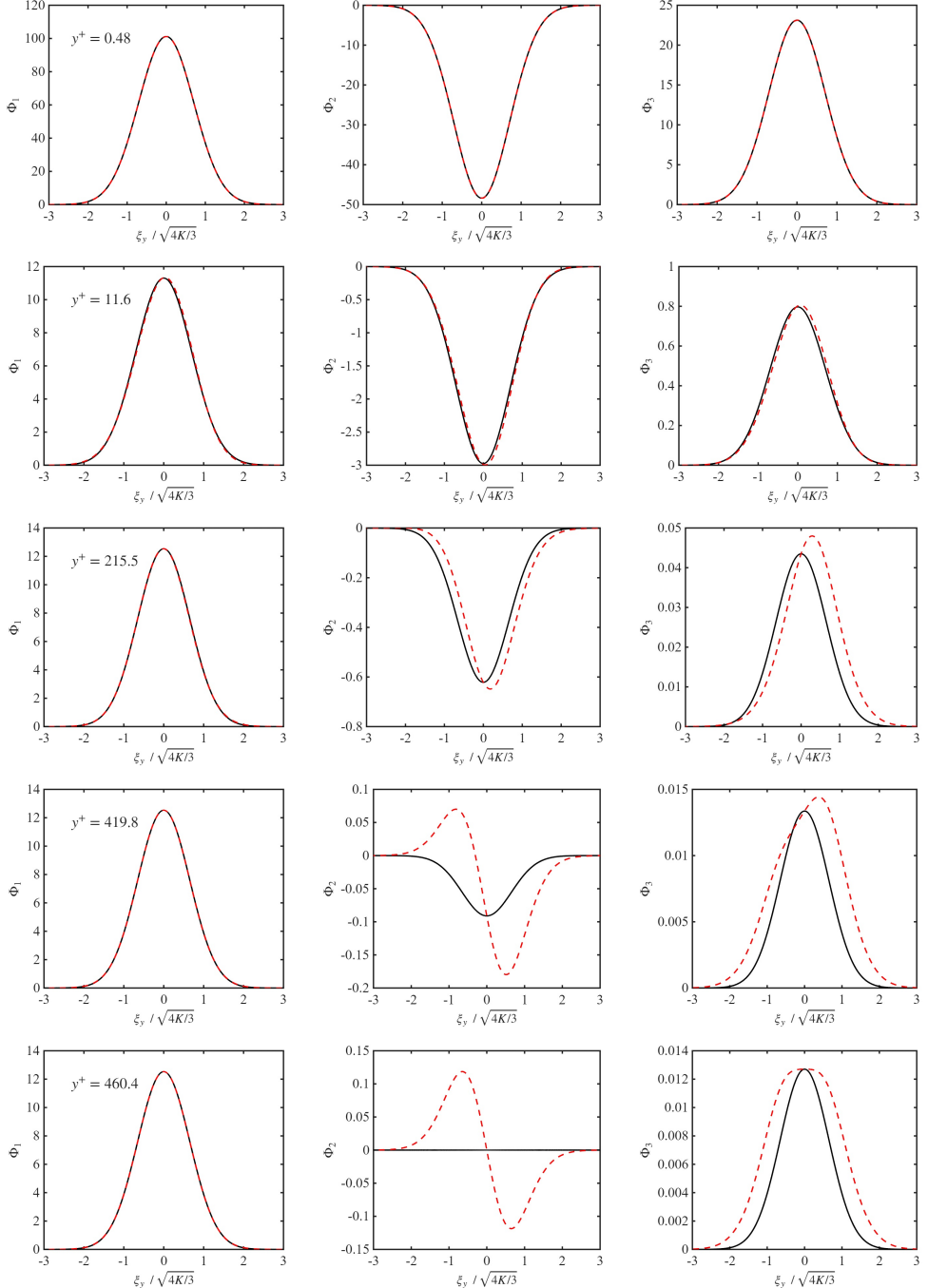


Figure 8: The reduced velocity distribution functions Φ_1 (first column), Φ_2 (second column) and Φ_3 (third column) from the LR-BGK model at $Re = 10133$ as a function of the microscopic velocity ξ_y at different wall-normal positions from top to bottom: $y^+ = 0.48$ (viscous sublayer), $y^+ = 11.6$ (buffer layer), $y^+ = 215.5$ (log-law region), $y^+ = 419.8$ (log-law region), and $y^+ = 460.4$ (channel centerline). Dash lines represent the computed distribution functions, while solid lines represent the local equilibrium distribution functions.

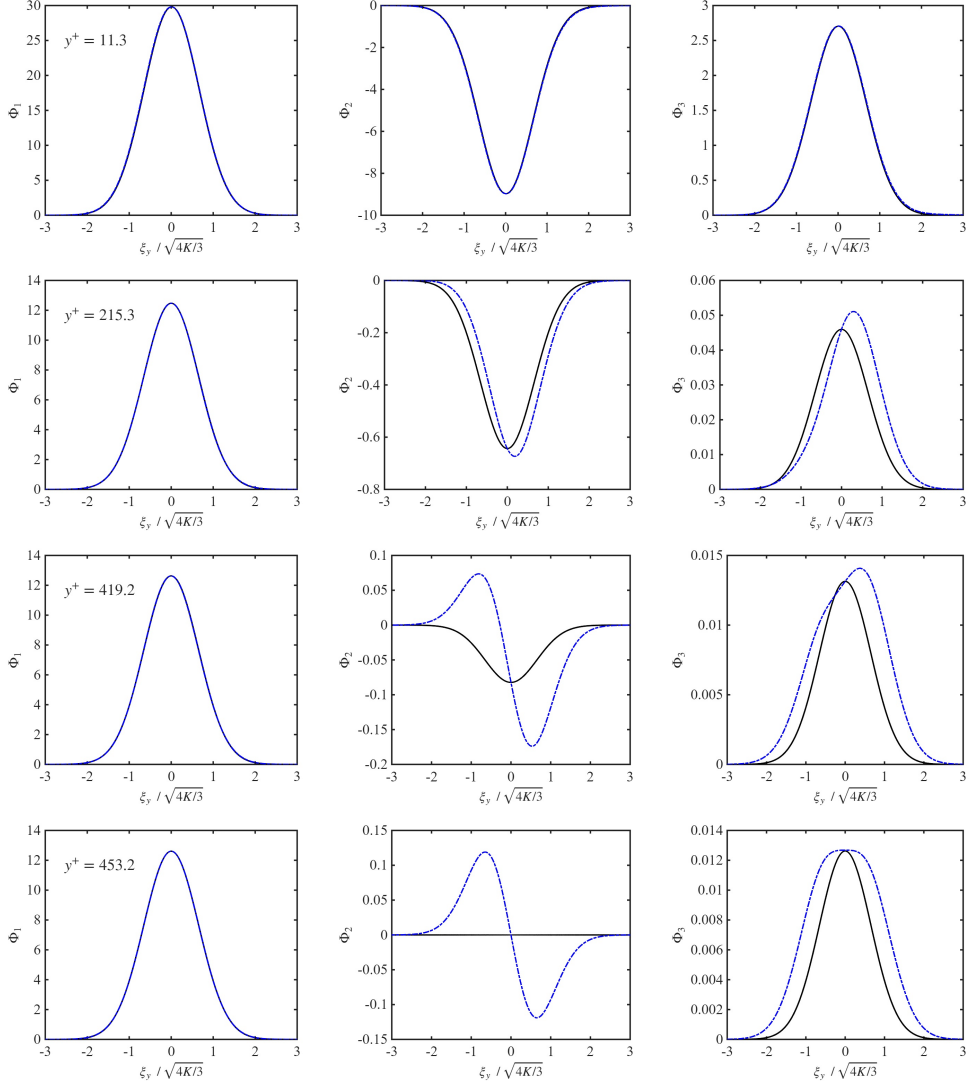


Figure 9: The reduced velocity distribution functions Φ_1 (first column), Φ_2 (second column) and Φ_3 (third column) from the HR-BGK model at $Re = 10133$ as a function of the microscopic velocity ξ_y at different wall-normal positions from top to bottom: $y^+ = 11.3$ (buffer layer), $y^+ = 215.3$ (log-law region), $y^+ = 419.2$ (log-law region), and $y^+ = 453.2$ (channel centerline). Dash-dot lines represent the computed distribution functions, while solid lines represent the local equilibrium distribution functions.

DNS data for turbulent plane Couette flow, demonstrating accurate prediction of mean velocity profiles, skin friction coefficients, and Reynolds stress distributions. They can capture essential flow physics including logarithmic law behaviour and Reynolds stress anisotropy. Although not as pronounced as indicated by DNS, the present kinetic theoretic models are shown to predict the separations between the normal stress components. In terms of predictive performance, the kinetic models achieve comparable accuracy to conventional nonlinear eddy viscosity models (Speziale 1987; Nisizima & Yoshizawa 1987; Myong & Kasagi 1990b; Craft et al. 1996) for mean

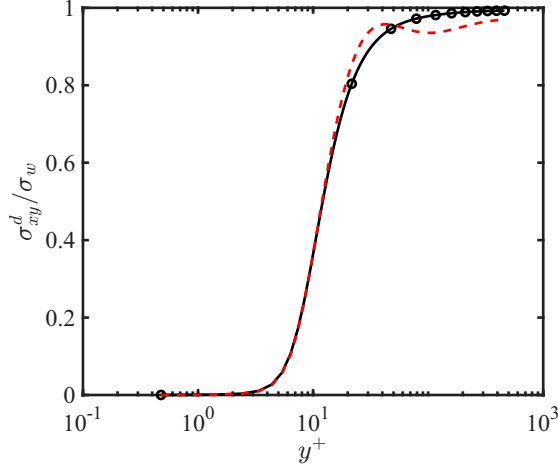


Figure 10: Deviatoric Reynolds shear stress component in wall units of turbulent Couette flow at $\text{Re} = 10133$. The solid lines with open circles and dash-dot lines represent the predictions of the LR-BGK model (5.9) and the CE expansion results (5.10), respectively. Here, the deviatoric Reynolds stress is defined as $\sigma^d = \sigma - \frac{1}{3}(\text{tr}\sigma)\mathbf{I}$.

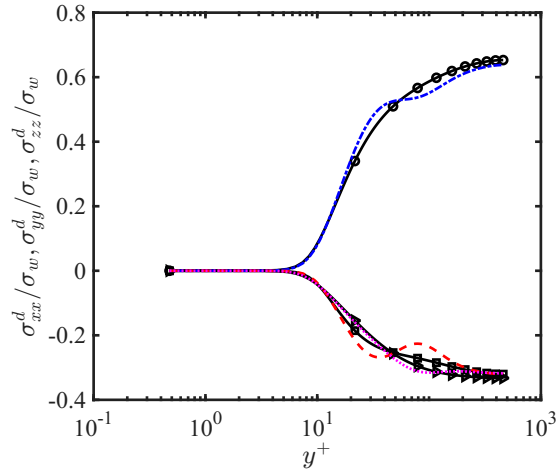


Figure 11: Deviatoric Reynolds normal stress components in wall units of turbulent Couette flow at $\text{Re} = 10133$. The solid lines with circles, squares, and triangles represent σ_{xx}^d , σ_{yy}^d , and σ_{zz}^d predicted by the LR-BGK model (5.9), respectively. The dash-dot, dash and dot lines represent σ_{xx}^d , σ_{yy}^d , and σ_{zz}^d predicted by the CE expansion results (5.10), respectively. Here, the deviatoric Reynolds stress is defined as $\sigma^d = \sigma - \frac{1}{3}(\text{tr}\sigma)\mathbf{I}$.

velocity profiles, skin friction coefficients, and Reynolds shear stress components. Nevertheless, accurate prediction of individual normal stress components in canonical wall-bounded flows remains a shared challenge. A distinctive advantage of the kinetic approach lies in its robust theoretical foundation, requiring only a single relaxation time, whereas nonlinear eddy viscosity models necessitate multiple *ad hoc* empirical coefficients for closure. These findings suggest that future developments should explore higher-order information about the collision term $C(F) \equiv -\nabla_\xi \cdot \langle \mathbf{a}' f' \rangle$ to achieve more accurate modelling of stress tensor anisotropy.

Analysis of the reduced velocity distribution functions revealed significant departures from local Gaussian equilibrium distribution, particularly for streamwise momentum and energy transport components. The non-equilibrium moments obtained from the kinetic model show excellent quantitative agreement with second-order Chapman-Enskog predictions, confirming the theoretical self-consistency of the approach. These non-equilibrium characteristics explain the ability of the kinetic model to capture non-Newtonian effects that linear eddy viscosity models cannot represent, highlighting the fundamental advantage of the kinetic approach over conventional turbulence modelling strategies.

Although this study focused on simple shear flows, the kinetic framework provides a foundation for modelling more complex turbulent phenomena. Future work should address three-dimensional flows, unsteady effects, and extension to compressible turbulence, fully exploiting the theoretical advantages of the kinetic approach. The kinetic turbulence model represents a significant step toward physics-based turbulence modelling, offering reduced dependence on empirical parameters while maintaining computational tractability for engineering applications. We wish to emphasize that the present work is to propose a kinetic theory based turbulence model, in the form of a Boltzmann-BGK differential equation, for better and more naturally capturing certain fundamental underlying physics of the averaged dynamics of turbulence, instead of a kinetic theory based computational method for numerically solving any turbulence problems

Acknowledgments

This work was supported by the National Natural Science Foundation of China (Grant No. 12472290) and the Interdisciplinary Research Program of HUST (2023JCYJ002). Z. Xin gratefully acknowledges the support of the China Scholarship Council (No. 202406160103). The computation is completed in the HPC Platform of Huazhong University of Science and Technology.

Declaration of interests

The authors report no conflict of interest.

Appendix A. Derivations of the Reynolds stress and turbulent kinetic energy flux via Chapman-Enskog expansion

In this Appendix, we provide a detailed derivation for the analytical expressions of the Reynolds stress tensor and TKE flux (namely (2.8)) via Chapman-Enskog expansion. The task involved in deriving a macroscopic representation of hydrodynamics is to express σ and Q in terms of the mean variables \mathbf{U} and K^{eq} , as well as their (spatial and temporal) derivatives. If the system is at equilibrium, it is straightforward to show that

$$\begin{aligned}\sigma_{\alpha\beta}^{eq} &= - \int (\xi_\alpha - U_\alpha) (\xi_\beta - U_\beta) F^{eq} d\xi = -\frac{2}{3} K^{eq} \delta_{\alpha\beta}, \\ Q_\alpha^{eq} &= \frac{1}{2} \int (\xi_\alpha - U_\alpha) (\xi_\beta - U_\beta)^2 F^{eq} d\xi = 0\end{aligned}\tag{A 1}$$

with

$$K^{eq} = \frac{1}{2} \int (\xi_\alpha - U_\alpha)^2 F^{eq} d\xi,\tag{A 2}$$

where $\delta_{\alpha\beta}$ is the Kronecker delta function. On the other hand, when there exists a flow involving non-trivial (spatial or temporal) inhomogeneities, there will be additional contributions to the stress tensor due to the non-equilibrium part of the distribution function, $F^{neq} = F - F^{eq}$. The

CE method is a systematic procedure to expand the velocity distribution function around its local equilibrium. This is possible if the ratio between the relaxation time τ and the representative advection time scale of the left hand side of (2.4) is small. Hence we may express the VDF in terms of a power series in \mathcal{K} :

$$F = F^{(0)} + \mathcal{K}F^{(1)} + \mathcal{K}^2F^{(2)} + \dots, \quad (\text{A } 3)$$

where $F^{(0)} = F^{eq}$, and the additional ($n > 0$) terms represent deviations from equilibrium at various orders in \mathcal{K} . These non-equilibrium corrections do contribute to the fluxes. For instance, the TKE, Reynolds stress and TKE flux from the n th order are given by

$$\begin{aligned} K^{(n)} &= \frac{1}{2} \int (\xi_\alpha - U_\alpha)^2 F^{(n)} d\xi, \\ \sigma_{\alpha\beta}^{(n)} &= - \int (\xi_\alpha - U_\alpha)(\xi_\beta - U_\beta) F^{(n)} d\xi, \\ Q_\alpha^{(n)} &= \frac{1}{2} \int (\xi_\alpha - U_\alpha)(\xi_\beta - U_\beta)^2 F^{(n)} d\xi. \end{aligned} \quad (\text{A } 4)$$

The CE expansion also requires expansion in time and space accordingly,

$$\partial_t = \mathcal{K}\partial_{t_1} + \mathcal{K}^2\partial_{t_2} + \dots, \quad \frac{\partial}{\partial x_\alpha} = \mathcal{K}\frac{\partial}{\partial x_{1\alpha}}, \quad (\text{A } 5)$$

and the force and strain rate tensor are similarly expanded as

$$\begin{aligned} \bar{a}_\alpha &= \mathcal{K}\bar{a}_\alpha^{(1)} + \mathcal{K}^2\bar{a}_\alpha^{(2)}, \quad \bar{a}_\alpha^{(1)} = -\frac{\partial \bar{p}}{\partial x_{1\alpha}}, \quad \bar{a}_\alpha^{(2)} = v_0 \nabla_1^2 U_\alpha, \\ S_{\alpha\beta} &= \mathcal{K}S_{\alpha\beta}^{(1)}, \quad S_{\alpha\beta}^{(1)} = \frac{1}{2} \left(\frac{\partial U_\alpha}{\partial x_{1\beta}} + \frac{\partial U_\beta}{\partial x_{1\alpha}} \right). \end{aligned} \quad (\text{A } 6)$$

Consequently, the kinetic equation (2.4) is turned into an infinite hierarchy of equations according to the order of \mathcal{K} ,

$$\sum_{k=1}^n \partial_{t_k} F^{(n-k)} + \xi_\alpha \frac{\partial F^{(n-1)}}{\partial x_{1\alpha}} + \sum_{k=1}^n \bar{a}_\alpha^{(k)} \frac{\partial F^{(n-k)}}{\partial \xi_\alpha} = -\frac{1}{\tau} F^{(n)}, \quad n = 1, 2, \dots, \infty. \quad (\text{A } 7)$$

In particular, for the first order ($n = 1$), we have,

$$\left(\partial_{t_1} + \xi_\alpha \frac{\partial}{\partial x_{1\alpha}} + \bar{a}_\alpha^{(1)} \frac{\partial}{\partial \xi_\alpha} \right) F^{eq} = -\frac{1}{\tau} F^{(1)}, \quad (\text{A } 8)$$

and for the second order ($n = 2$),

$$\left(\partial_{t_1} + \xi_\alpha \frac{\partial}{\partial x_{1\alpha}} + \bar{a}_\alpha^{(1)} \frac{\partial}{\partial \xi_\alpha} \right) F^{(1)} + \partial_{t_2} F^{eq} + \bar{a}_\alpha^{(2)} \frac{\partial F^{eq}}{\partial \xi_\alpha} = -\frac{1}{\tau} F^{(2)}. \quad (\text{A } 9)$$

The fastest time derivative ∂_{t_1} corresponding to isotropic turbulence is a result of the equilibrium VDF:

$$\begin{aligned} \frac{\partial U_\alpha}{\partial x_{1\alpha}} &= 0, \\ \partial_{t_1} U_\alpha + U_\beta \frac{\partial U_\alpha}{\partial x_{1\beta}} &= -\frac{\partial \bar{p}}{\partial x_{1\alpha}} - \frac{\partial}{\partial x_{1\beta}} \left(\frac{2}{3} K^{eq} \delta_{\alpha\beta} \right), \\ \partial_{t_1} K^{eq} + U_\alpha \frac{\partial K^{eq}}{\partial x_{1\alpha}} &= -\frac{K^{(1)}}{\tau}. \end{aligned} \quad (\text{A } 10)$$

Since the space-time dependence in F^{eq} is only obtained through U_α and K^{eq} , we have

$$\begin{aligned} \left(\partial_{t_1} + \xi_\alpha \frac{\partial}{\partial x_{1\alpha}} + \bar{a}_\alpha^{(1)} \frac{\partial}{\partial \xi_\alpha} \right) F^{eq} &= \frac{\partial F^{eq}}{\partial U_\beta} \left(\partial_{t_1} + \xi_\alpha \frac{\partial}{\partial x_{1\alpha}} \right) U_\beta \\ &\quad + \frac{\partial F^{eq}}{\partial K^{eq}} \left(\partial_{t_1} + \xi_\alpha \frac{\partial}{\partial x_{1\alpha}} \right) K^{eq} + \bar{a}_\alpha^{(1)} \frac{\partial F^{eq}}{\partial \xi_\alpha}. \end{aligned} \quad (\text{A 11})$$

Using the equilibrium VDF (2.11), it can be shown directly that

$$\begin{aligned} \frac{\partial F^{eq}}{\partial U_\beta} &= \frac{3(\xi_\beta - U_\beta)}{2K^{eq}} F^{eq}, \\ \frac{\partial F^{eq}}{\partial K^{eq}} &= \frac{3}{2K^{eq}} \left(\frac{(\xi_\alpha - U_\alpha)^2}{2K^{eq}} - 1 \right) F^{eq}, \\ \frac{\partial F^{eq}}{\partial \xi_\alpha} &= -\frac{3(\xi_\alpha - U_\alpha)}{2K^{eq}} F^{eq}, \end{aligned} \quad (\text{A 12})$$

and then combining (A 8)-(A 12), we obtain

$$\begin{aligned} F^{(1)} &= -\tau \left(\partial_{t_1} + \xi_\alpha \frac{\partial}{\partial x_{1\alpha}} + \bar{a}_\alpha^{(1)} \frac{\partial}{\partial \xi_\alpha} \right) F^{eq} \\ &= -\frac{3\tau(\xi_\alpha - U_\alpha)}{2K^{eq}} \left(\frac{(\xi_\alpha - U_\alpha)^2}{2K^{eq}} - \frac{5}{3} \right) \frac{\partial K^{eq}}{\partial x_{1\alpha}} F^{eq} \\ &\quad + \frac{3K^{(1)}}{2K^{eq}} \left(\frac{(\xi_\alpha - U_\alpha)^2}{2K^{eq}} - 1 \right) F^{eq} - \frac{3\tau(\xi_\alpha - U_\alpha)(\xi_\beta - U_\beta)}{2K^{eq}} \frac{\partial U_\alpha}{\partial x_{1\beta}} F^{eq}. \end{aligned} \quad (\text{A 13})$$

Substituting (A 13) into the stress and TKE flux moments, and after some straightforward algebra, it can be shown that

$$\begin{aligned} \sigma_{\alpha\beta}^{(1)} &= -\frac{2}{3} K^{(1)} \delta_{\alpha\beta} + \frac{4\tau K^{eq}}{3} S_{\alpha\beta}^{(1)}, \\ Q_\alpha^{(1)} &= -\frac{10}{9} \tau K^{eq} \frac{\partial K^{eq}}{\partial x_{1\alpha}}. \end{aligned} \quad (\text{A 14})$$

Furthermore, we present a derivation for the second-order CE expansion in the rest of this Appendix. Using the result of the first-order derivation above, we obtain the hydrodynamic time derivative at the first order. That is,

$$\begin{aligned} \partial_{t_2} U_\alpha &= \frac{2}{3} \frac{\partial}{\partial x_{1\beta}} \left[2\tau K^{eq} S_{\alpha\beta}^{(1)} - K^{(1)} \delta_{\alpha\beta} \right] + v_0 \nabla_1^2 U_\alpha, \\ \partial_{t_1} K^{(1)} + \partial_{t_2} K^{eq} &= \frac{\partial}{\partial x_{1\alpha}} \left[\frac{10}{9} \tau K^{eq} \frac{\partial K^{eq}}{\partial x_{1\alpha}} - U_\alpha K^{(1)} \right] + \frac{4\tau K^{eq}}{3} S_{\alpha\beta}^{(1)} S_{\alpha\beta}^{(1)} - \frac{K^{(2)}}{\tau}. \end{aligned} \quad (\text{A 15})$$

This is a direct result of the CE expansion up to the first order. Based on (A 9), (A 12) and (A 13), together with

$$\partial_{t_2} F^{eq} = \frac{\partial F^{eq}}{\partial U_\beta} \partial_{t_2} U_\beta + \frac{\partial F^{eq}}{\partial K^{eq}} \partial_{t_2} K^{eq}, \quad (\text{A 16})$$

and it is easy to obtain

$$\begin{aligned} \partial_{t_2} F^{eq} = & \frac{3F^{eq}}{2K^{eq}} \left\{ \frac{2(\xi_\alpha - U_\alpha)}{3} \left[\frac{\partial}{\partial x_{1\beta}} \left(2\tau K^{eq} S_{\alpha\beta}^{(1)} \right) - \frac{\partial K^{(1)}}{\partial x_{1\alpha}} + v_0 \nabla_1^2 U_\alpha \right] + \left(\frac{(\xi_\alpha - U_\alpha)^2}{2K^{eq}} - 1 \right) \right. \\ & \times \left. \left[\frac{\partial}{\partial x_{1\alpha}} \left(\frac{10}{9} \tau K^{eq} \frac{\partial K^{eq}}{\partial x_{1\alpha}} \right) - U_\alpha \frac{\partial K^{(1)}}{\partial x_{1\alpha}} - \partial_{t_1} K^{(1)} - \frac{K^{(2)}}{\tau} + \frac{4\tau K^{eq}}{3} S_{\alpha\beta}^{(1)} S_{\beta\alpha}^{(1)} \right] \right\}. \end{aligned} \quad (\text{A 17})$$

Combining (A 9), (A 10), (A 13), and (A 17), we have

$$\begin{aligned} \sigma_{\alpha\beta}^{(2)} = & - \int (\xi_\alpha - U_\alpha) (\xi_\beta - U_\beta) F^{(2)} d\xi \\ = & - \frac{2K^{(2)}}{3} \delta_{\alpha\beta} - \frac{4\tau}{3K^{eq}} \left(\partial_{t_1} + U_\gamma \frac{\partial}{\partial x_\gamma} \right) \left[\tau (K^{eq})^2 S_{\alpha\beta}^{(1)} \right] \\ & - \frac{8\tau^2 K^{eq}}{3} \left(S_{\alpha\gamma}^{(1)} S_{\gamma\beta}^{(1)} - \frac{1}{3} \delta_{\alpha\beta} S_{\gamma\eta}^{(1)} S_{\gamma\eta}^{(1)} \right) + \frac{4\tau^2 K^{eq}}{3} \left(S_{\alpha\gamma}^{(1)} \Omega_{\gamma\beta}^{(1)} + S_{\beta\gamma}^{(1)} \Omega_{\gamma\alpha}^{(1)} \right) \\ & - \frac{4\tau}{9} \left[\frac{\partial}{\partial x_{1\beta}} \left(\tau K^{eq} \frac{\partial K^{eq}}{\partial x_{1\alpha}} \right) + \frac{\partial}{\partial x_{1\alpha}} \left(\tau K^{eq} \frac{\partial K^{eq}}{\partial x_{1\beta}} \right) - \frac{2}{3} \delta_{\alpha\beta} \frac{\partial}{\partial x_{1\gamma}} \left(\tau K^{eq} \frac{\partial K^{eq}}{\partial x_{1\gamma}} \right) \right], \end{aligned} \quad (\text{A 18})$$

and

$$\begin{aligned} Q_\alpha^{(2)} = & \frac{1}{2} \int (\xi_\alpha - U_\alpha) (\xi_\beta - U_\beta)^2 F^{(2)} d\xi \\ = & \frac{10\tau}{9K^{eq}} \left(\partial_{t_1} + U_\gamma \frac{\partial}{\partial x_\gamma} \right) \left[\tau (K^{eq})^2 \frac{\partial K^{eq}}{\partial x_{1\alpha}} \right] + \frac{10\tau^2 K^{eq}}{9} \frac{\partial K^{eq}}{\partial x_{1\beta}} \frac{\partial U_\beta}{\partial x_{1\alpha}} \\ & - \frac{5\tau K^{eq}}{3} \frac{\partial}{\partial x_{1\beta}} \left(\frac{4\tau K^{eq}}{3} S_{\alpha\beta}^{(1)} \right) + \frac{5\tau K^{eq}}{3} a_\alpha^{(1)}, \end{aligned} \quad (\text{A 19})$$

where $\Omega_{\alpha\beta}$ is the vorticity tensor of the mean velocity field, which is defined as

$$\Omega_{\alpha\beta} \equiv \frac{1}{2} \left(\frac{\partial U_\alpha}{\partial x_\beta} - \frac{\partial U_\beta}{\partial x_\alpha} \right) = \mathcal{K} \Omega_{\alpha\beta}^{(1)}, \quad \Omega_{\alpha\beta}^{(1)} = \frac{1}{2} \left(\frac{\partial U_\alpha}{\partial x_{1\beta}} - \frac{\partial U_\beta}{\partial x_{1\alpha}} \right). \quad (\text{A 20})$$

Appendix B. The discretized velocity method of the kinetic model for (quasi-one-dimensional) turbulent Couette flow

Since only a quasi-one-dimensional turbulent Couette flow is considered in this study, four reduced VDFs are introduced to cast the three-dimensional velocity space (ξ_x, ξ_y, ξ_z) into one dimension as

$$\begin{aligned} \Phi_1(y, \xi_y, t) &= \int F(\mathbf{x}, \boldsymbol{\xi}, t) d\xi_x d\xi_z, \\ \Phi_2(y, \xi_y, t) &= \int \xi_x F(\mathbf{x}, \boldsymbol{\xi}, t) d\xi_x d\xi_z, \\ \Phi_3(y, \xi_y, t) &= \int \xi_x^2 F(\mathbf{x}, \boldsymbol{\xi}, t) d\xi_x d\xi_z, \\ \Phi_4(y, \xi_y, t) &= \int \xi_z^2 F(\mathbf{x}, \boldsymbol{\xi}, t) d\xi_x d\xi_z. \end{aligned} \quad (\text{B 1})$$

Then the mean variables can be computed by taking moments of the reduced VDFs,

$$\begin{aligned} U_x(y, t) &= \int \Phi_2 d\xi_y, & U_y(y, t) &= \int \xi_y \Phi_1 d\xi_y, \\ K(y, t) &= \frac{1}{2} \int \left((\xi_y - U_y)^2 \Phi_1 + \Phi_3 - U_x^2 \Phi_1 + \Phi_4 \right) d\xi_y - U_x^2, \end{aligned} \quad (\text{B } 2)$$

and the high-order moments of interest are given by

$$\begin{aligned} \sigma_{xx}(y, t) &= - \int \left(\Phi_3 - U_x^2 \Phi_1 \right) d\xi_y + 2U_x^2, \\ \sigma_{xy}(y, t) &= - \int \xi_y \Phi_2 d\xi_y + U_x U_y, \\ \sigma_{yy}(y, t) &= - \int (\xi_y - U_y)^2 \Phi_1 d\xi_y, \\ \sigma_{zz}(y, t) &= - \int \Phi_4 d\xi_y. \end{aligned} \quad (\text{B } 3)$$

Without loss of generality, we present the discretized velocity method for the LR-BGK model (4.5) and (4.7). The governing equations for the four reduced VDFs can be deduced as

$$\partial_t \Phi_\alpha + \xi_y \frac{\partial \Phi_\alpha}{\partial y} = \frac{\Phi_\alpha^{eq} - \Phi_\alpha}{\tau} + S_\alpha, \quad \alpha = 1, 2, 3, 4, \quad (\text{B } 4)$$

where Φ_α^{eq} are the reduced equilibrium VDFs,

$$\begin{aligned} \Phi_1^{eq} &= \left(\frac{4}{3} \pi K^{eq} \right)^{-\frac{1}{2}} \exp \left[- \frac{3 (\xi_y - U_y)^2}{4 K^{eq}} \right], \\ \Phi_2^{eq} &= U_x \Phi_1^{eq}, \quad \Phi_3^{eq} = \left(\frac{2 K^{eq}}{3} + U_x^2 \right) \Phi_1^{eq}, \quad \Phi_4^{eq} = \frac{2 K^{eq}}{3} \Phi_1^{eq}, \end{aligned} \quad (\text{B } 5)$$

and S_α represent the corresponding source terms,

$$\begin{aligned} S_1 &= -\bar{a}_y \frac{\partial \Phi_1}{\partial \xi_y} - \frac{\nu_0 \nabla^2 K}{2 K^{eq}} \left(\Phi_1 + (\xi_y - U_y) \frac{\partial \Phi_1}{\partial \xi_y} \right), \\ S_2 &= \bar{a}_x \Phi_1 - \bar{a}_y \frac{\partial \Phi_2}{\partial \xi_y} - \frac{\nu_0 \nabla^2 K}{2 K^{eq}} \left(U_x \Phi_1 + (\xi_y - U_y) \frac{\partial \Phi_2}{\partial \xi_y} \right), \\ S_3 &= 2\bar{a}_x \Phi_2 - \bar{a}_y \frac{\partial \Phi_3}{\partial \xi_y} - \frac{\nu_0 \nabla^2 K}{2 K^{eq}} \left(U_x \Phi_2 - \Phi_3 + (\xi_y - U_y) \frac{\partial \Phi_3}{\partial \xi_y} \right), \\ S_4 &= -\bar{a}_y \frac{\partial \Phi_4}{\partial \xi_y} - \frac{\nu_0 \nabla^2 K}{2 K^{eq}} \left(-\Phi_4 + (\xi_y - U_y) \frac{\partial \Phi_4}{\partial \xi_y} \right). \end{aligned} \quad (\text{B } 6)$$

Within the finite-volume framework, the governing equation (B 4) for Φ_α is discretized as

$$\Phi_{\alpha,j}^{n+1} = \Phi_{\alpha,j}^n - \frac{\xi_y \Delta t}{\Delta y} \left(\Phi_{\alpha,j+1/2}^{n+1/2} - \Phi_{\alpha,j-1/2}^{n+1/2} \right) + \frac{\Delta t}{\tau^{n+1}} \left(\Phi_{\alpha,j}^{eq,n+1} - \Phi_{\alpha,j}^{n+1} \right) + \Delta t S_{\alpha,j}^n, \quad (\text{B } 7)$$

where $\Delta y = y_{j+1/2} - y_{j-1/2}$ is the length of the cell j , $\Phi_{j-1/2}^{n+1/2}$ and $\Phi_{j+1/2}^{n+1/2}$ are the left and right VDFs at the cell interface at time $t^{n+1/2}$, respectively.

To eliminate the implicit collision term, we introduce the transformed VDFs

$$\tilde{\Phi}_\alpha = \Phi_\alpha - \frac{\Delta t}{\tau} (\Phi_\alpha^{eq} - \Phi_\alpha), \quad (\text{B } 8)$$

and the mean variables can be computed by taking moments of the transformed VDFs,

$$\begin{aligned} U_x &= \int \tilde{\Phi}_2 d\xi_y, & U_y &= \int \xi_y \tilde{\Phi}_1 d\xi_y, \\ K &= \frac{1}{2} \int \left((\xi_y - U_y)^2 \tilde{\Phi}_1 + \tilde{\Phi}_3 - U_x^2 \tilde{\Phi}_1 + \tilde{\Phi}_4 \right) d\xi_y - U_x^2 - \Delta t \epsilon. \end{aligned} \quad (\text{B 9})$$

Then equation (B 7) can be rewritten as

$$\tilde{\Phi}_{\alpha,j}^{n+1} = \Phi_{\alpha,j}^n - \frac{\xi_y \Delta t}{\Delta y} \left(\Phi_{\alpha,j+1/2}^{n+1/2} - \Phi_{\alpha,j-1/2}^{n+1/2} \right) + \Delta t S_{\alpha,j}^n, \quad (\text{B 10})$$

where the mean pressure entering the source term is governed by the kinematic pressure–Poisson relation $\frac{\partial^2 \tilde{p}^n}{\partial y^2} = \frac{\partial^2 \sigma_{yy}^n}{\partial y^2}$.

As a result, the original VDFs and the mean variables at t^{n+1} can be obtained from $\tilde{\Phi}_{\alpha,j}^{n+1}$ according to (B 8) and (B 9),

$$\begin{aligned} \Phi_{\alpha,j}^{n+1} &= \frac{\tau}{\tau + \Delta t} \tilde{\Phi}_{\alpha,j}^{n+1} + \frac{\Delta t}{\tau + \Delta t} \Phi_{\alpha,j}^{eq,n+1}, \\ U_{x,j}^{n+1} &= \int \tilde{\Phi}_{2,j}^{n+1} d\xi_y, \\ U_{y,j}^{n+1} &= \int \xi_y \tilde{\Phi}_{1,j}^{n+1} d\xi_y, \\ K_j^{n+1} &= \frac{1}{2} \int \left((\xi_y - U_{y,j}^{n+1})^2 \tilde{\Phi}_{1,j}^{n+1} + \tilde{\Phi}_{3,j}^{n+1} - U_x^2 \tilde{\Phi}_{1,j}^{n+1} + \tilde{\Phi}_{4,j}^{n+1} \right) d\xi_y - \left(U_{x,j}^{n+1} \right)^2 - \Delta t \epsilon_j^{n+1}. \end{aligned} \quad (\text{B 11})$$

and σ_j^{n+1} are calculated by the original VDFs $\Phi_{\alpha,j}^{n+1}$ according to (B 3).

The governing equation (5.3) for ϵ is also discretized using the finite-volume method,

$$\begin{aligned} \epsilon_j^{n+1} &= \epsilon_j^n + \frac{\Delta t}{\Delta y} \left(\frac{v_T}{C_\epsilon} \left(\frac{\partial \epsilon}{\partial y} \right)_{j+1/2}^n - U_{j+1/2}^n \epsilon_{j+1/2}^n - \frac{v_T}{C_\epsilon} \left(\frac{\partial \epsilon}{\partial y} \right)_{j-1/2}^n + U_{j-1/2}^n \epsilon_{j-1/2}^n \right) \\ &\quad + C_{\epsilon 1} \frac{\epsilon_j^n}{K_j^n} \left(\sigma_{xy,j}^n \left(\frac{\partial U_x}{\partial y} \right)_j^n + \sigma_{yy,j}^n \left(\frac{\partial U_y}{\partial y} \right)_j^n \right) - C_{\epsilon 2} f_{\epsilon 2} \frac{(\epsilon_j^n)^2}{K_j^n}, \end{aligned} \quad (\text{B 12})$$

where the velocity gradient is evaluated using a central finite difference. Thus, the update rules for the VDFs and the macroscopic variables are given by equations (B 10), (B 11) and (B 12); the remaining task is to reconstruct the VDFs and macroscopic variables at interface.

First, the VDFs at cell interface are reconstructed from the local solution of the collisionless kinetic equations (B 4),

$$\Phi_\alpha(y_{j+1/2}, \xi_y, t^{n+1/2}) = \Phi_\alpha(y_{j+1/2} - \xi_y \Delta t / 2, \xi_y, t^n). \quad (\text{B 13})$$

With the Taylor expansion around the cell interface $y_{j+1/2}$, for smooth flows, $\Phi_\alpha(y_{j+1/2}, \xi_y, t^{n+1/2})$ can be approximated by linear interpolations,

$$\Phi_\alpha(y_{j+1/2}, \xi_y, t^{n+1/2}) = \Phi_\alpha(y_{j+1/2}, \xi_y, t^n) - \frac{\xi_y \Delta t}{2} \frac{\Phi_\alpha(y_{j+1}, \xi_y, t^n) - \Phi_\alpha(y_j, \xi_y, t^n)}{y_{j+1} - y_j}, \quad (\text{B 14})$$

and

$$\Phi_\alpha(y_{j+1/2}, \xi_y, t^n) = \Phi_\alpha(y_j, \xi_y, t^n) + (y_{j+1/2} - y_j) \frac{\Phi_\alpha(y_{j+1}, \xi_y, t^n) - \Phi_\alpha(y_j, \xi_y, t^n)}{y_{j+1} - y_j}. \quad (\text{B 15})$$

Then, the mean variables and ϵ at the cell interface are also obtained by linear interpolation,

$$\begin{aligned} U_{j+1/2}^n &= U_j^n + (y_{j+1/2} - y_j) \frac{U_{j+1}^n - U_j^n}{y_{j+1} - y_j}, \\ K_{j+1/2}^n &= K_j^n + (y_{j+1/2} - y_j) \frac{K_{j+1}^n - K_j^n}{y_{j+1} - y_j}, \\ \epsilon_{j+1/2}^n &= \epsilon_j^n + (y_{j+1/2} - y_j) \frac{\epsilon_{j+1}^n - \epsilon_j^n}{y_{j+1} - y_j}, \\ \left(\frac{\partial \epsilon}{\partial y} \right)_{j+1/2}^n &= (y_{j+1/2} - y_j) \frac{\epsilon_{j+1}^n - \epsilon_j^n}{y_{j+1} - y_j}. \end{aligned} \quad (\text{B } 16)$$

Additionally, this model still contains compressibility errors during time evolution. Here, we introduce a correction to the mean pressure defined by (B 7). That is, the flow velocity is

$$U_{y,j}^{n*} = U_{y,j}^n - \frac{\Delta t}{\Delta y} \left(\int \xi_y^2 \Phi_{1,j+1/2}^{n+1/2} d\xi_y - \int \xi_y^2 \Phi_{1,j-1/2}^{n+1/2} d\xi_y \right) + \Delta t \left(- \left(\frac{\partial \bar{p}}{\partial y} \right)_j^n + \left(v_0 \nabla^2 U \right)_j^n \right). \quad (\text{B } 17)$$

Further, we define the pressure correction as the difference between the updated and the previous pressure field $\delta \bar{p} \equiv \bar{p}_j^{n+1} - \bar{p}_j^n$. With this definition, the corrected velocity field is expressed as

$$U_{y,j}^{n+1} = U_{y,j}^{n*} - \Delta t \frac{\partial(\delta \bar{p})}{\partial y}. \quad (\text{B } 18)$$

In order to enforce $U_{y,j}^{n+1}$ to be divergent free, δp should satisfy the following Poisson equation,

$$\frac{\partial^2(\delta \bar{p})}{\partial y^2} = \frac{1}{\Delta t} \frac{\partial U_{y,j}^{n*}}{\partial y}. \quad (\text{B } 19)$$

After solving the above equation, one can obtain the fluid velocity $U_{y,j}^{n+1}$.

The above method is valid in a continuous velocity space ξ_y . In practical computations, the velocity space is divided into a finite set of discrete velocities $\{\xi_{y,k} \mid k = 1, 2, \dots, N\}$, where N is the number of discrete velocities. It is important to discretize the velocity space based on certain quadrature rules, which are chosen according to the rarefaction degree. The gradients of VDFs in the source term are approximated by central differences,

$$\left(\frac{\partial \Phi_\alpha}{\partial \xi_y} \right)_k = \frac{\Phi_\alpha(\xi_{y,k+1}) - \Phi_\alpha(\xi_{y,k-1})}{(\xi_{y,k+1} - \xi_{y,k-1})}. \quad (\text{B } 20)$$

The discrete velocity method described above is similar to the well-known discrete unified gas kinetic scheme (Guo et al. 2013), with the only difference being that the construction of the interface distribution function does not take into account collision effects. For completeness, the general algorithmic framework consists of the following steps:

- (i) At the initial time ($n = 0$), the variables $(U^0, K^0$ and $\epsilon^0)$ and the original VDFs Φ_α^0 are initialized at each cell center;
- (ii) Evolve the VDFs Φ_α at each cell interface at time $t^{n+1/2}$ according to (B 14) and (B 15), and then calculate the mean variables and ϵ at each cell interface according to (B 16);
- (iii) Update ϵ^{n+1} at each cell interface according to (B 12);
- (iv) Update the transformed VDFs $\tilde{\Phi}_\alpha^{n+1}$, and then update VDFs Φ_α^{n+1} and mean variables U^{n+1} and K^{n+1} using (B 11);
- (v) Correct the mean velocity $U_{y,j}^{n+1}$ according to (B 17), (B 18), and (B 19);
- (vi) Advance the time step ($n \rightarrow n + 1$) and repeat step (ii) to (v) until the end.

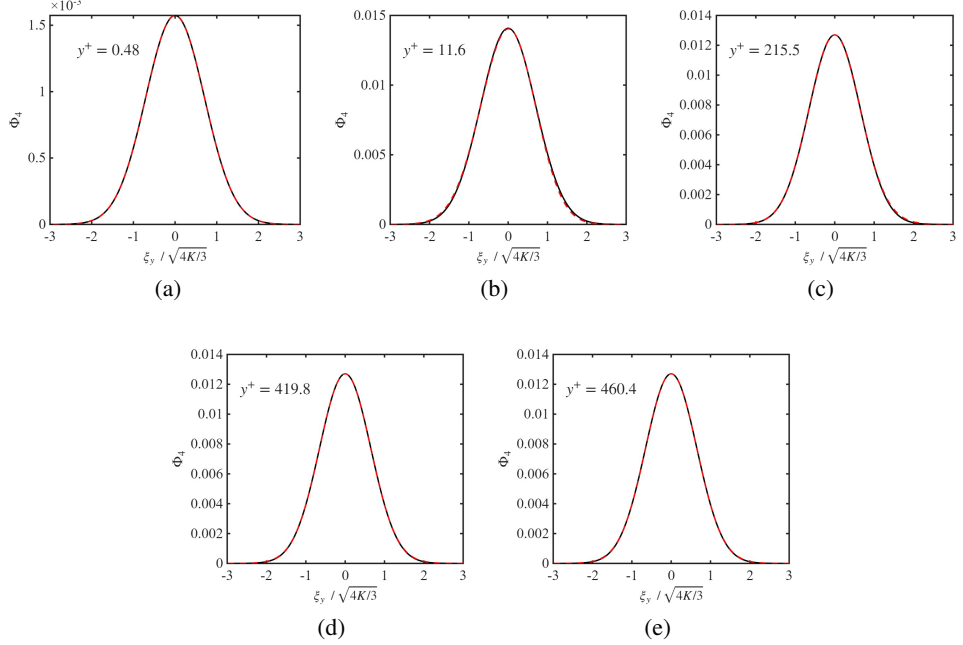


Figure 12: The reduced velocity distribution function Φ_4 from the LR-BGK at $\text{Re} = 10133$ as a function of the microscopic velocity ξ_y scaled by local parameters $\sqrt{4K/3}$ at different wall-normal positions from top to bottom: (a) $y^+ = 0.48$, (b) $y^+ = 11.6$, (c) $y^+ = 215.5$, (d) $y^+ = 419.8$, and (e) $y^+ = 460.4$. Dash lines represent the computed distribution functions, while solid lines represent the local equilibrium distribution functions.

Appendix C. The Reduced distribution function Φ_4 from kinetic model

The fourth reduced distribution function Φ_4 , which represents the vertical Reynolds normal stress component, exhibits a behaviour similar to Φ_1 , remaining essentially in equilibrium across all wall-normal position.

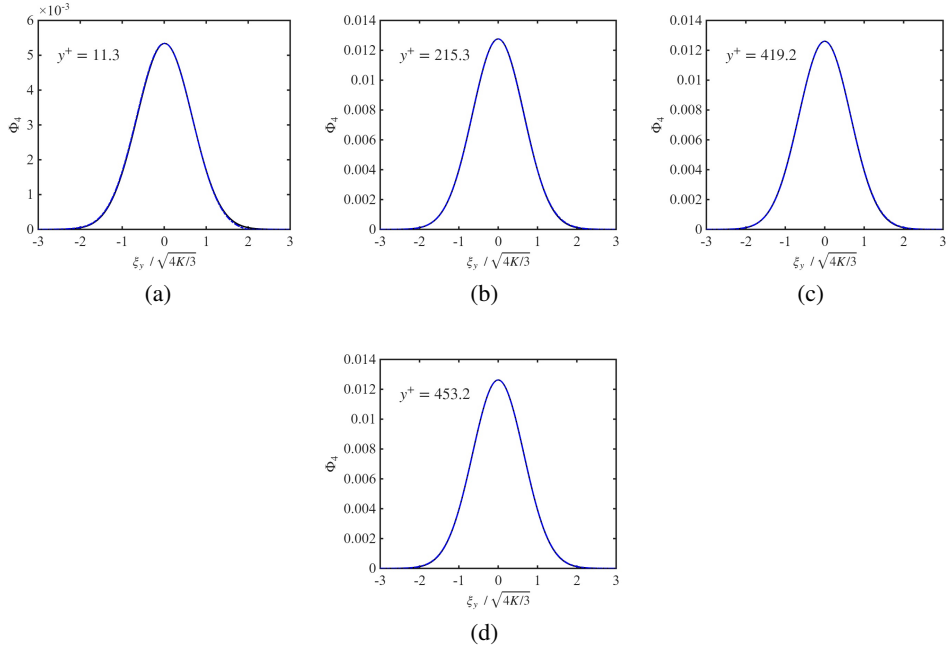


Figure 13: The reduced velocity distribution function Φ_4 from the HR-BGK model at $\text{Re} = 10133$ as a function of the microscopic velocity ξ_y scaled by local parameters $\sqrt{4K/3}$ at different wall-normal positions from top to bottom: (a) $y^+ = 11.3$, (b) $y^+ = 215.3$, (c) $y^+ = 419.2$, and (d) $y^+ = 453.2$. Dash lines represent the computed distribution functions, while solid lines represent the local equilibrium distribution functions.

REFERENCES

ANDERSSON, HI & PETTERSSON, BA 1994 Modeling plane turbulent Couette flow. *International Journal of Heat and Fluid Flow* **15** (6), 447–455.

ANSUMALI, SANTOSH, KARLIN, ILIYA V & SUCCI, SAURO 2004 Kinetic theory of turbulence modeling: smallness parameter, scaling and microscopic derivation of Smagorinsky model. *Physica A* **338** (3-4), 379–394.

AOKI, KAZUO, GIOVANGIGLI, VINCENT & KOSUGE, SHINGO 2022 Boundary conditions for the Boltzmann equation from gas-surface interaction kinetic models. *Physical Review E* **106** (3), 035306.

BASU, SUKANTA & HOLTSLAG, ALBERT AM 2021 Turbulent Prandtl number and characteristic length scales in stably stratified flows: steady-state analytical solutions. *Environmental Fluid Mechanics* **21** (6), 1273–1302.

BECH, KNUT H, TILLMARK, NILS, ALFREDSSON, P HENRIK & ANDERSSON, HELGE I 1995 An investigation of turbulent plane Couette flow at low Reynolds numbers. *Journal of Fluid Mechanics* **286**, 291–325.

BHATNAGAR, PRABHU LAL, GROSS, EUGENE P & KROOK, MAX 1954 A model for collision processes in gases. i. small amplitude processes in charged and neutral one-component systems. *Physical Review* **94** (3), 511.

CERCIGNANI, CARLO 1972 Scattering kernels for gas-surface interactions. *Transport Theory and Statistical Physics* **2** (1), 27–53.

CERCIGNANI, CARLO 1988 The Boltzmann equation. In *The Boltzmann Equation and Its Applications*, pp. 40–103. Springer.

CERCIGNANI, CARLO & LAMPIS, MARIA 1971 Kinetic models for gas-surface interactions. *Transport Theory and Statistical Physics* **1** (2), 101–114.

CHANDRA, LALTU & GRÖTZBACH, GÜNTHER 2007 Analysis and modeling of the turbulent diffusion of turbulent kinetic energy in natural convection. *Flow, Turbulence and Combustion* **79**, 133–154.

CHAPMAN, SYDNEY & COWLING, THOMAS GEORGE 1990 *The Mathematical Theory of Non-Uniform Gases*. Cambridge University Press.

CHEN, HUODONG, KANDASAMY, SATHEESH, ORSZAG, STEVEN, SHOCK, RICK, SUCCI, SAURO & YAKHOT, VICTOR 2003 Extended Boltzmann kinetic equation for turbulent flows. *Science* **301** (5633), 633–636.

CHEN, HUODONG, ORSZAG, STEVEN A, STAROSELSKY, ILYA & SUCCI, SAURO 2004 Expanded analogy between Boltzmann kinetic theory of fluids and turbulence. *Journal of Fluid Mechanics* **519**, 301–314.

CHEN, HUODONG, STAROSELSKY, ILYA, SREENIVASAN, KATEPALLI R & YAKHOT, VICTOR 2023 Average turbulence dynamics from a one-parameter kinetic theory. *Atmosphere* **14** (7), 1109.

CHEN, HUODONG, STAROSELSKY, ILYA, SREENIVASAN, KATEPALLI R & YAKHOT, VICTOR 2024 Average turbulence dynamics from a one-parameter kinetic theory: Estimation of the relaxation time. *Physics of Fluids* **36** (3), 035156.

CHEN, HUODONG, SUCCI, SAURO & ORSZAG, STEVEN 1999 Analysis of subgrid scale turbulence using the Boltzmann Bhatnagar-Gross-Krook kinetic equation. *Physical Review E* **59** (3), R2527.

COHEN, EZECHIEL GODERT DAVID & BALAZS, NANDOR L 1962 Fundamental problems in statistical mechanics. *Physics Today* **15** (12), 64–66.

CRAFT, TJ, LAUNDER, BE & SUGA, K 1996 Development and application of a cubic eddy-viscosity model of turbulence. *International Journal of Heat and Fluid Flow* **17** (2), 108–115.

DURBIN, PAUL A 2018 Some recent developments in turbulence closure modeling. *Annual Review of Fluid Mechanics* **50** (1), 77–103.

EL TELBANY, MMM & REYNOLDS, AJ 1980 Velocity distributions in plane turbulent channel flows. *Journal of Fluid Mechanics* **100** (1), 1–29.

FRISCH, URIEL 1996 *Turbulence*. Cambridge University Press.

GATSKI, THOMAS B & SPEZIALE, CHARLES G 1993 On explicit algebraic stress models for complex turbulent flows. *Journal of Fluid Mechanics* **254**, 59–78.

GIRIMAJI, SHARATH S 2007 Boltzmann kinetic equation for filtered fluid turbulence. *Physical Review Letters* **99** (3), 034501.

GRÖTZBACH, G 1982 Direct numerical simulation of the turbulent momentum and heat transfer in an internally heated fluid layer. *Heat Transfer* **2**, 141–146.

GUO, ZHAOLI, XU, KUN & WANG, RUIJIE 2013 Discrete unified gas kinetic scheme for all Knudsen number flows: Low-speed isothermal case. *Physical Review E* **88** (3), 033305.

GUO, ZHAOLI, ZHENG, CHUGUANG & SHI, BAOCHANG 2002 Non-equilibrium extrapolation method for velocity and pressure boundary conditions in the lattice Boltzmann method. *Chinese Physics* **11** (4), 366.

HAMINGTON, PETER E & DAHM, WERNER JA 2008 Reynolds stress closure for nonequilibrium effects in turbulent flows. *Physics of Fluids* **20** (11), 115101.

HANJALIĆ, K & LAUNDER, BRIAN EDWARD 1976 Contribution towards a Reynolds-stress closure for low-Reynolds-number turbulence. *Journal of Fluid Mechanics* **74** (4), 593–610.

HEINZ, STEFAN 2007 Unified turbulence models for LES and RANS, FDF and PDF simulations. *Theoretical and Computational Fluid Dynamics* **21**, 99–118.

HENRY, FS & REYNOLDS, AJ 1984 Analytical solution of two gradient-diffusion models applied to turbulent Couette flow. *ASME Journal of Fluids Engineering* **106** (2), 211–216.

JONES, W PETER & LAUNDER, BRIAN EDWARD 1972 The prediction of laminarization with a two-equation model of turbulence. *International Journal of Heat and Mass Transfer* **15** (2), 301–314.

KAYS, WILLIAM M 1994 Turbulent Prandtl number. where are we? *ASME Journal of Heat Transfer* **116** (2), 284–295.

KITO, OSAMI, NAKABYASHI, KOICHI & NISHIMURA, FUTOSHI 2005 Experimental study on mean velocity and turbulence characteristics of plane Couette flow: low-Reynolds-number effects and large longitudinal vortical structure. *Journal of Fluid Mechanics* **539**, 199–227.

KLIMONTOVICH, YU L 1969 The statistical theory of non-equilibrium processes in a plasma. *Journal of Plasma Physics* **3**, 148.

KOSUGE, SHINGO, AOKI, KAZUO, GIOVANGIGLI, VINCENT & GOLSE, FRANÇOIS 2025 Applications of new boundary conditions for the Boltzmann equation derived from a kinetic model of gas-surface interaction. *Physical Review Fluids* **10** (5), 053401.

LAUNDER, BRIAN EDWARD, REECE, G JR & RODI, W 1975 Progress in the development of a Reynolds-stress turbulence closure. *Journal of Fluid Mechanics* **68** (3), 537–566.

LAUNDER, BRIAN EDWARD & SHARMA, BAHRAT I 1974 Application of the energy-dissipation model of

turbulence to the calculation of flow near a spinning disc. *Letters in Heat and Mass Transfer* **1** (2), 131–137.

LAUNDER, BRIAN EDWARD & SPALDING, DUDLEY BRIAN 1983 The numerical computation of turbulent flows. In *Numerical Prediction of Flow, Heat Transfer, Turbulence and Combustion*, pp. 96–116. Elsevier.

LORD, RG 1991 Some extensions to the Cercignani-Lampis gas-surface scattering kernel. *Physics of Fluids A* **3** (4), 706–710.

LUAN, PENG, ZHANG, HAOFUAN & ZHANG, JUN 2025 Constructing turbulence models using the kinetic Fokker–Planck equation. *Journal of Fluid Mechanics* **1011**, A44.

LUNDGREN, TS 1967 Distribution functions in the statistical theory of turbulence. *Physics of Fluids* **10** (5), 969–975.

LUNDGREN, TS 1969 Model equation for nonhomogeneous turbulence. *Physics of Fluids* **12** (3), 485–497.

MAXWELL, JAMES CLERK 1879 VII. On stresses in rarefied gases arising from inequalities of temperature. *Philosophical Transactions of the Royal Society of London* (170), 231–256.

MENTER, FLORIAN R 1997 Eddy viscosity transport equations and their relation to the k - ε model. *ASME Journal of Fluids Engineering* **119** (4), 876–884.

MOENG, CHIN-HOH & WYNGAARD, JOHN C 1989 Evaluation of turbulent transport and dissipation closures in second-order modeling. *Journal of Atmospheric Sciences* **46** (14), 2311–2330.

MOIN, PARVIZ & MAHESH, KRISHNAN 1998 Direct numerical simulation: a tool in turbulence research. *Annual Review of Fluid Mechanics* **30** (1), 539–578.

MONIN, ANDRE SERGEEVICH & YAGLOM, AKIVA M 2013 *Statistical Fluid Mechanics, Volume II: Mechanics of Turbulence*. Courier Corporation.

MYONG, HYON KOOK & KASAGI, NOBUHIDE 1990a A new approach to the improvement of k - ε turbulence model for wall-bounded shear flows. *JSME International Journal Ser. 2* **33** (1), 63–72.

MYONG, HYON KOOK & KASAGI, NOBUHIDE 1990b Prediction of anisotropy of the near-wall turbulence with an anisotropic low-Reynolds-number k - ε turbulence model. *ASME Journal of Fluids Engineering* **112**, 521–524.

NAGANO, Y & TAGAWA, M 1990 An improved k - ε model for boundary layer flows. *ASME Journal of Fluids Engineering* **112** (1), 33–39.

NISIZIMA, SHOITI & YOSHIZAWA, AKIRA 1987 Turbulent channel and Couette flows using an anisotropic k - ε model. *AIAA Journal* **25** (3), 414–420.

PIROZZOLI, SERGIO, BERNARDINI, MATTEO & ORLANDI, PAOLO 2014 Turbulence statistics in Couette flow at high Reynolds number. *Journal of Fluid Mechanics* **758**, 327–343.

POPE, STEPHEN B 1975 A more general effective-viscosity hypothesis. *Journal of Fluid Mechanics* **72** (2), 331–340.

POPE, STEPHEN B 2001 Turbulent flows. *Measurement Science and Technology* **12** (11), 2020–2021.

PRANDTL, LUDWIG 1925 über die ausgebildete turbulenz. *Zeitschrift für angewandte Mathematik und Mechanik* **5**, 136–139, in German.

REICHARDT, H 1956 Über die geschwindigkeitsverteilung in einer geradlinigen turbulenten couetteströmung. *ZAMM-Journal of Applied Mathematics and Mechanics/Zeitschrift für Angewandte Mathematik und Mechanik* **36** (S1), S26–S29.

REYNOLDS, OSBORNE 1895 IV. On the dynamical theory of incompressible viscous fluids and the determination of the criterion. *Philosophical Transactions of the Royal Society of London.(a.)* (186), 123–164.

ROBERTSON, JAMES M 1959a On turbulent plane Couette flow. In *Proc. 6th Midwestern Conf. on Fluid Mech.*, University of Texas, Austin, pp. 169–182.

ROBERTSON, JAMES M 1959b *A Study of Turbulent Plane Couette Flow*. University of Illinois, Department of Theoretical and Applied Mechanics.

RUBINSTEIN, ROBERT & BARTON, J MICHAEL 1990 Nonlinear Reynolds stress models and the renormalization group. *Physics of Fluids A* **2** (8), 1472–1476.

SCHNEIDER, W 1989 On Reynolds stress transport in turbulent Couette flow. *Zeitschrift für Flugwissenschaften und Weltraumforschung* **13**, 315–319.

SHAKHOV, EM 1968 Generalization of the Krook kinetic relaxation equation. *Fluid Dynamics* **3** (5), 95–96.

SPALART, PHILIPPE & ALLMARAS, STEVEN 1992 A one-equation turbulence model for aerodynamic flows. In *30th Aerospace Sciences Meeting and Exhibit*, p. 439.

SPEZIALE, CHARLES G 1987 On nonlinear k - l and k - ε models of turbulence. *Journal of Fluid Mechanics* **178**, 459–475.

SREENIVASAN, KATEPALLI R & YAKHOT, VICTOR 2021 Dynamics of three-dimensional turbulence from Navier-Stokes equations. *Physical Review Fluids* **6** (10), 104604.

SREENIVASAN, KATEPALLI R, YAKHOT, VICTOR, STAROSELISKY, ILYA & CHEN, HUODONG 2024 Saturation of exponents and the asymptotic fourth state of turbulence. *Physical Review Research* **6** (3), 033087.

SRINIVASAN, R, GIDDENS, DP, BANGERT, LH & WU, JC 1977 Turbulent plane Couette flow using probability distribution functions. *The Physics of Fluids* **20** (4), 557–567.

SUTTON, OLIVER GRAHAM 2020 Atmospheric Turbulence. Routledge.

TAVOULARIS, STAVROS & CORRSIN, STANLEY 1981 Experiments in nearly homogenous turbulent shear flow with a uniform mean temperature gradient. Part 1. *Journal of Fluid Mechanics* **104**, 311–347.

TENNEKES, HENDRIK & LUMLEY, JOHN LEASK 1972 A First Course in Turbulence. MIT Press.

TSUKAHARA, TAKAHIRO, KAWAMURA, HIROSHI & SHINGAI, KENJI 2006 DNS of turbulent Couette flow with emphasis on the large-scale structure in the core region. *Journal of Turbulence* (7), N19.

VENUGOPAL, VISHNU, PRATURI, DIVYA SRI & GIRIMAJI, SHARATH S 2019 Non-equilibrium thermal transport and entropy analyses in rarefied cavity flows. *Journal of Fluid Mechanics* **864**, 995–1025.

WALLIN, STEFAN & JOHANSSON, ARNE V 2000 An explicit algebraic Reynolds stress model for incompressible and compressible turbulent flows. *Journal of Fluid Mechanics* **403**, 89–132.

WILCOX, DAVID C 1998 Turbulence Modeling for CFD. DCW Industries.

WILCOX, DAVID C 2008 Formulation of the $k-\omega$ turbulence model revisited. *AIAA Journal* **46** (11), 2823–2838.

WU, LEI, REESE, JASON M & ZHANG, YONGHAO 2014 Solving the Boltzmann equation deterministically by the fast spectral method: application to gas microflows. *Journal of Fluid Mechanics* **746**, 53–84.

XU, KUN, LIU, HONGWEI & JIANG, JIANZHENG 2007 Multiple-temperature kinetic model for continuum and near continuum flows. *Physics of Fluids* **19** (1), 016101.

YAKHOT, VSASTBCG, ORSZAG, STEVEN A, THANGAM, SIVA, GATSKI, TB & SPEZIALE, CG 1992 Development of turbulence models for shear flows by a double expansion technique. *Physics of Fluids A* **4** (7), 1510–1520.

YANG, XIAOJIAN & XU, KUN 2025 Wave-particle based multiscale modeling and simulation of non-equilibrium turbulent flows. *arXiv preprint arXiv:2503.07207* .

YOSHIZAWA, AKIRA & NISIZIMA, SHOITI 1993 A nonequilibrium representation of the turbulent viscosity based on a two-scale turbulence theory. *Physics of Fluids A* **5** (12), 3302–3304.